



**HAL**  
open science

## **Cdc123, a Cell Cycle Regulator Needed for eIF2 Assembly, Is an ATP-Grasp Protein with Unique Features**

Michel Panvert, Etienne Dubiez, Lea Arnold, Javier Perez, Yves Mechulam,  
Wolfgang Seufert, Emmanuelle Schmitt

► **To cite this version:**

Michel Panvert, Etienne Dubiez, Lea Arnold, Javier Perez, Yves Mechulam, et al.. Cdc123, a Cell Cycle Regulator Needed for eIF2 Assembly, Is an ATP-Grasp Protein with Unique Features. *Structure*, 2015, 23 (9), pp.1596-1608. 10.1016/j.str.2015.06.014 . hal-01222821

**HAL Id: hal-01222821**

**<https://polytechnique.hal.science/hal-01222821>**

Submitted on 30 Oct 2015

**HAL** is a multi-disciplinary open access archive for the deposit and dissemination of scientific research documents, whether they are published or not. The documents may come from teaching and research institutions in France or abroad, or from public or private research centers.

L'archive ouverte pluridisciplinaire **HAL**, est destinée au dépôt et à la diffusion de documents scientifiques de niveau recherche, publiés ou non, émanant des établissements d'enseignement et de recherche français ou étrangers, des laboratoires publics ou privés.

1  
2  
3 Cdc123, a cell cycle regulator needed for eIF2 assembly,  
4  
5 is an ATP-grasp protein with unique features  
6  
7  
8  
9  
10  
11  
12  
13

14 Michel Panvert<sup>1</sup>, Etienne Dubiez<sup>1</sup>, Lea Arnold<sup>2</sup>, Javier Perez<sup>3</sup>, Yves Mechulam<sup>1</sup>,  
15  
16 Wolfgang Seufert<sup>\*2</sup> and Emmanuelle Schmitt<sup>1\*</sup>  
17  
18  
19  
20  
21  
22  
23  
24  
25  
26  
27  
28  
29  
30  
31

32 <sup>1</sup>Laboratoire de Biochimie, Ecole Polytechnique, CNRS, F-91128 Palaiseau cedex, France. Phone : +33-  
33 1-69334485; Fax: +33-1-69334909  
34  
35

36 <sup>2</sup>Department of Genetics, University of Regensburg, D-93040 Regensburg, Germany, Phone : +49-941-  
37 943-3162; Fax: +49-941-943-3163  
38  
39

40 <sup>3</sup>SOLEIL Synchrotron, L'Orme des Merisiers, F-91190 Saint Aubin, France  
41  
42  
43

44  
45 \*Co-corresponding authors: [emma@bioc.polytechnique.fr](mailto:emma@bioc.polytechnique.fr) and [Wolfgang.Seufert@ur.de](mailto:Wolfgang.Seufert@ur.de)  
46  
47  
48  
49  
50

51 "The authors declare that they have no conflict of interest."  
52

53 Running title: Cdc123 is an ATP-grasp protein  
54  
55  
56  
57  
58  
59  
60  
61  
62  
63  
64  
65

1 **ABSTRACT**

2  
3  
4 Eukaryotic initiation factor 2 (eIF2), a heterotrimeric GTPase, has a central role in protein  
5 biosynthesis by supplying methionylated initiator tRNA to the ribosomal translation initiation complex  
6 and by serving as a target for translational control in response to stress. Recent work identified a novel  
7 step indispensable for eIF2 function: assembly of eIF2 from its three protein subunits by the cell  
8 proliferation protein Cdc123. We report the first crystal structure of a Cdc123 representative, that from  
9 *Schizosaccharomyces pombe*, both isolated and bound to the domain III of eIF2 $\gamma$  from *Saccharomyces*  
10 *cerevisiae*. The structures show that Cdc123 resembles enzymes of the ATP-grasp family. Indeed,  
11 Cdc123 binds ATP-Mg<sup>2+</sup> and conserved residues contacting ATP-Mg<sup>2+</sup> are essential for Cdc123 to  
12 support eIF2 assembly and cell viability. A docking of eIF2 $\alpha\gamma$  onto Cdc123, combined with genetic  
13 and biochemical experiments, allows us to propose a model explaining how Cdc123 participates in the  
14 biogenesis of eIF2 through facilitating assembly of eIF2 $\gamma$  to eIF2 $\alpha$ .  
15  
16  
17  
18  
19  
20  
21  
22  
23  
24  
25  
26  
27  
28  
29  
30  
31  
32  
33  
34  
35  
36  
37  
38  
39  
40  
41  
42  
43  
44  
45  
46  
47  
48  
49  
50  
51  
52  
53  
54  
55  
56  
57  
58  
59  
60  
61  
62  
63  
64  
65

## INTRODUCTION

1  
2 Initiation of the translation of a messenger RNA into a protein involves a complex cascade of  
3  
4 molecular events, leading to a translation-competent ribosome with a methionylated initiator tRNA in  
5  
6 the P-site, base-paired with the start codon on mRNA (Hinnebusch, 2011; Lorsch and Dever, 2010). A  
7  
8 critical consequence of the whole process is the setting of the reading frame for mRNA decoding. In  
9  
10 eukaryotic and archaeal cells, the initiator tRNA carrier is the e/aIF2 heterotrimer. e/aIF2 results from  
11  
12 the association of three subunits,  $\alpha$ ,  $\beta$  and  $\gamma$ . The  $\gamma$  subunit forms the core of the heterotrimer. It  
13  
14 interacts with both the  $\alpha$  and the  $\beta$  subunits while  $\alpha$  and  $\beta$  do not interact together (Schmitt et al.,  
15  
16 2010). In its GTP-bound form, this factor specifically binds Met-tRNA<sub>i</sub><sup>Met</sup> (Schmitt et al., 2012) and  
17  
18 handles it in the initiation complex (Huang et al., 1997). After start codon recognition, the factor, in its  
19  
20 GDP-bound form, loses affinity for Met-tRNA<sub>i</sub><sup>Met</sup> and eventually dissociates from the initiation  
21  
22 complex (Algire et al., 2005). This leaves Met-tRNA<sub>i</sub><sup>Met</sup> in the P site of the small ribosomal subunit  
23  
24 and allows the final steps of initiation to occur. In this process, specific handling of the initiator tRNA  
25  
26 by e/aIF2 and control of the nucleotide state of the factor are crucial for accuracy.  
27  
28  
29  
30

31  
32 According to its central role in translation, eIF2 was early identified as a central target in  
33  
34 response to stress conditions (Gebauer and Hentze, 2004; Holcik and Sonenberg, 2005). Such  
35  
36 conditions trigger phosphorylation of the  $\alpha$  subunit of the heterotrimer that, in turn, leads eIF2 to form  
37  
38 an inactive complex with the guanine nucleotide exchange factor eIF2B. The subsequent sequestering  
39  
40 of eIF2 reprograms gene expression by both reducing global translation and specifically enhancing the  
41  
42 translation of mRNAs encoding activators of the transcription of stress adaptation genes (Hinnebusch,  
43  
44 2005).  
45  
46

47  
48 Proteomic studies in *S. cerevisiae* have reported interaction of the  $\gamma$  subunit of eIF2 with the  
49  
50 cell proliferation protein Cdc123 (*e.g.* (Ho et al., 2002)). This gene was first identified in mammals as  
51  
52 the target of mutations blocking the G1-S transition in the cell cycle (Ohno et al., 1984; Okuda and  
53  
54 Kimura, 1996). In human, CDC123 was described as a candidate oncogene in breast cancer (Adelaide  
55  
56 et al., 2007) and implicated in other diseases (Soler Artigas et al., 2011; Zeggini et al., 2008).  
57  
58

59 Relationships between eIF2 and Cdc123 became clearer when it was shown that assembly of the eIF2  
60  
61  
62  
63  
64  
65

1  
2  
3  
4  
5  
6  
7  
8  
9  
10  
11  
12  
13  
14  
15  
16  
17  
18  
19  
20  
21  
22  
23  
24  
25  
26  
27  
28  
29  
30  
31  
32  
33  
34  
35  
36  
37  
38  
39  
40  
41  
42  
43  
44  
45  
46  
47  
48  
49  
50  
51  
52  
53  
54  
55  
56  
57  
58  
59  
60  
61  
62  
63  
64  
65

complex *in vivo* depended on Cdc123 (Perzmaier et al., 2013). Indeed, mutations of Cdc123 in budding yeast reduced the association of the eIF2 subunits, diminished polysome levels, and increased *GCN4* expression indicating that Cdc123 was critical for eIF2 activity. Using co-immunoprecipitation from *S. cerevisiae* cell extracts as well as pull-down experiments with *E. coli* expressed proteins, an interaction between Cdc123 and the unassembled  $\gamma$  subunit of eIF2 was shown (Perzmaier et al., 2013). More precisely, the results have indicated that domain III of the  $\gamma$  subunit of eIF2 was required for binding to Cdc123. Alterations of the binding site revealed a strict correlation between Cdc123 binding, the biological function of eIF2 $\gamma$  and its ability to assemble with  $\alpha$  and  $\beta$  subunits. Overexpression of Cdc123 neutralized the eIF2 assembly defect. Moreover, overexpression of eIF2  $\alpha$  or  $\gamma$  subunits rescued an otherwise inviable *cdc123* deletion mutant with a strong synergistic effect when both  $\alpha$  and  $\gamma$  subunits were overproduced. In contrast, overexpression of eIF2 $\beta$  could not compensate for the absence of Cdc123. Thus, Cdc123 has appeared as an essential protein acting as a specific assembly factor of the eIF2 heterotrimeric complex by promoting the eIF2 $\alpha\gamma$  assembly step (Perzmaier et al., 2013). The requirement of Cdc123 in eukaryotes may explain why all attempts to produce isolated yeast eIF2 $\gamma$  were unsuccessful (Naveau et al., 2013).

Here, we report the first crystal structure of a Cdc123 representative, that from *Schizosaccharomyces pombe*, both isolated and bound to the domain III of eIF2 $\gamma$  ( $\gamma$ DIII) from *Saccharomyces cerevisiae*. Cdc123 resembles enzymes of the ATP-grasp family and indeed binds ATP-Mg<sup>2+</sup>. Structural data and biochemical studies revealed that ATP-Mg<sup>2+</sup> is needed for Cdc123 activity. A docking of eIF2 $\alpha\gamma$  onto Cdc123 allows us to propose a tentative model explaining how Cdc123 participates in the biogenesis of eIF2 through facilitating assembly of eIF2 $\gamma$  to eIF2 $\alpha$ .

## RESULTS

### *Overall structure of Sp-Cdc123*

Despite many attempts, no crystal could be obtained using Cdc123 from *S. cerevisiae* (Sc-Cdc123). Therefore, we have chosen to purify Cdc123 from *Schizosaccharomyces pombe*, Sp-Cdc123. Indeed, the two proteins share 35% identities (55% similarities). Moreover, Sp-Cdc123 is shorter than Sc-Cdc123 (319 amino acids as compared to 360 in the case of Sc-Cdc123) with smaller predicted loop regions ((Cole et al., 2008); Figure S1A). Various crystal forms of full-length Sp-Cdc123 were obtained (Table S1). The 3D structure was solved using anomalous scattering data from crystals of selenomethionylated Cdc123, combined with non-crystallographic symmetry and multi-crystal averaging. The initial density map allowed us to trace most of the C $\alpha$  backbone and to identify non-crystallographic symmetry operators. This permitted partial refinement of a first 3D model of Sp-Cdc123 at 3.24 Å resolution. This model contained residues 2-271 with the exception of residues 51 to 71. The C-terminal part of the protein (272 to 319) was not visible in the electron density. We suspected that mobility of this region within the crystals might have hampered the diffraction quality. Therefore, a C-terminal truncated form of Sp-Cdc123 (1 to 274, hereafter named Sp-Cdc123 $\Delta$ c) was engineered. High-resolution diffracting crystals could be obtained using Sp-Cdc123 $\Delta$ c (Table 1). The structure was solved by molecular replacement using the 3.24 Å resolution model and refined to 2.06 Å resolution. Final statistics are given in Table 1. The final model contains two monomers of Sp-Cdc123 $\Delta$ c in the asymmetric unit. As in the case of the model obtained with the full-length protein, residues 51 to 71 were not defined in the electron density for both monomers and loop 148-152 was difficult to model. Notably, the C-terminally truncated protein and the full-length protein were arranged as a tetramer within the crystals. Nevertheless, Sp-Cdc123 behaved as a monomer in solution, as shown by molecular sieving and SEC-MALS (see Experimental Procedures).

The structure of Sp-Cdc123 $\Delta$ c monomer can be divided into two  $\alpha$ - $\beta$  domains. The N-terminal domain contains residues 2 to 170 (domain 1) and the central domain contains residues 171 to 274 (domain 2, Figure 1). A comparison of the Sp-Cdc123 structure to other known structures was performed using the Dali server (Holm and Sander, 1995). All high scoring entries in the PDB

1 belonged to the ATP-grasp family. Representative top scoring matches are shown figure S2B. All  
2 homologous structures shown in Figure S2B can be aligned to Cdc123 with Z-scores ranging from 8.3  
3 to 11.2 and rmsd in the 3 Å range for 156-179 aligned residues. ATP-grasp enzymes catalyze similar  
4 reactions, involving an ATP-dependent ligation of a carboxyl group carbon with an amino or imino  
5 group nitrogen. Catalysis proceeds, in each case, through the formation of an acylphosphate  
6 intermediate (Artymiuk et al., 1996; Fan et al., 1995; Galperin and Koonin, 1997). This homology was  
7 unanticipated according to the low sequence similarities of Cdc123 with proteins of the ATP-grasp  
8 family (in the 10% range, Figure S2) and had previously not been detected using standard BLAST  
9 procedures. The classical ATP-grasp fold is formed of three domains usually named, N, central and C  
10 domains (or A, B and C (Fawaz et al., 2011)). The N domains are not structurally conserved between  
11 the various ATP-grasp enzymes. Comparison of ATP-grasp enzymes with Cdc123 (Figures 2 and S2)  
12 shows, however, that the structural homology is restricted to the central and C domains (equivalent to  
13 domains 1 and 2 in Cdc123, respectively; Figure 2C). Indeed, the N terminal domain of ATP-grasp  
14 enzymes (colored gray in Figure S2B) is not observed in Cdc123 proteins. Domain 1 of Cdc123  
15 contains a three-stranded  $\beta$ -sheet, whereas the corresponding  $\beta$ -sheet in ATP-grasp enzymes contains  
16 a fourth strand (Figure 2B). Residues forming this additional strand are inserted between  $\beta$ 2 and  $\beta$ 3  
17 counterparts of Cdc123 domain 1 (Figure S2A). Domain 2 of Cdc123 contains a four-stranded  
18 antiparallel  $\beta$ -sheet with a topology similar to that observed in the C-terminal domain of ATP-grasp  
19 enzymes (Figure S2). A fifth  $\beta$ -strand is observed at the C-terminal part of Cdc123 $\Delta$ c. Finally, within  
20 domains 1 and 2, regions specific to Cdc123 are inserted or divergent (colored green in Figure 2 and in  
21 Figure S2). Among these are regions involved in ATP binding in grasp enzymes (colored orange in  
22 Figures 2 and S2 (Fan et al., 1995)).

23  
24  
25  
26  
27  
28  
29  
30  
31  
32  
33  
34  
35  
36  
37  
38  
39  
40  
41  
42  
43  
44  
45  
46  
47  
48  
49  
50  
51  
52  
53  
54  
55  
56  
57  
58  
59  
60  
61  
62  
63  
64  
65

Despite these differences, the obvious resemblance of Cdc123 with ATP-grasp enzymes suggested that Cdc123 had the ability to bind ATP.

*Cdc123 binds ATP*

1  
2 As an attempt to evidence ATP binding by Sp-Cdc123, a titration of the protein with ATP was  
3 followed using ITC (Experimental Procedures). A dissociation constant of  $67 \pm 13 \mu\text{M}$  could be  
4 deduced from the titration curve (Figure S3). This  $K_d$  value is in the same range as that measured for a  
5 typical ATP-grasp enzyme, the *S. aureus* D-alanine:D-alanine ligase ( $60\mu\text{M}$ , Liu et al., 2006). This  
6 result shows that Sp-Cdc123 indeed binds ATP with significant affinity.  
7  
8  
9

10  
11 In order to obtain further insight into ATP binding, crystallization trials with Sp-Cdc123 $\Delta\text{c}$   
12 were performed in the presence of ATP-Mg<sup>2+</sup>, AMP-PNP-Mg<sup>2+</sup> and ADP-Mg<sup>2+</sup>. Crystals isomorphic  
13 to crystals with unliganded Sp-Cdc123 $\Delta\text{c}$  were obtained and datasets were collected. However, a  
14 bound nucleotide was only observed when crystals were prepared in the presence of AMP-PNP. In  
15 this case, there was no density for the  $\gamma$ -phosphate group in the maps and therefore the density was  
16 assigned to an ADP molecule. Instability of AMP-PNP in acidic conditions has been reported (Sigma-  
17 Aldrich product information sheet) and could explain the presence of ADP instead of AMP-PNP. Only  
18 one ADP molecule bound to monomer A was clearly identified (Table 1, Figure 3). No magnesium  
19 ion bound to ADP was observed. In monomer B, residual electron density within the pocket was  
20 attributed to water molecules. Their positions may reflect low occupancy of ADP. Possibly, packing  
21 constraints may have hampered tight binding of ADP to the second monomer.  
22  
23  
24  
25  
26  
27  
28  
29  
30  
31  
32  
33  
34

35  
36 In monomer A, ADP is bound in a position corresponding to the ATP binding pocket  
37 previously identified in ATP-grasp enzymes, at the interface between the domain 1 and domain 2  
38 (Figures 1 and 2). One side of the ADP molecule is held by residues located in domain 2 of Cdc123,  
39 belonging to motifs conserved in all ATP-grasp enzymes (yellow residues in  $\beta 4$ - $\beta 7$ , Figure 3A). At  
40 the opposite side, some residues belonging to domain 1 participate in the binding of ADP (residues  
41 164-167, blue residues in Figure 3A). Additional contacts involve residues located in non-conserved  
42 regions (residues 99, 101, 103, colored green in Figure 3A). Interestingly, the two regions  
43 corresponding to the loops involved in ATP binding in ATP-grasp enzymes, named “small loop” and  
44 “large loop” (Figure 2B and S2, residues 176-180 and 233-261 in 1E4E), are highly divergent in  
45 Cdc123. These two regions of ATP-grasp enzymes form a lid in the presence of ATP, interacting  
46 together above the ATP binding cavity (Figure 2B and S2 (Fan et al., 1995; Hara et al., 1996; Roper et  
47 al., 2000; Zhao et al., 2013)). In place of the small loop segment, region 98-110 contains stretches of  
48  
49  
50  
51  
52  
53  
54  
55  
56  
57  
58  
59  
60  
61  
62  
63  
64  
65

1 residues highly conserved in Cdc123 proteins (Figure S1). Finally, comparison of the structure of  
2 unliganded Cdc123 with that of ADP-bound Cdc123 only showed adjustments of side chains involved  
3  
4 in the binding of ADP.  
5

6 Overall, analysis of the ADP binding site in Cdc123 shows that nucleotide binding involves  
7  
8 regions and residues of the protein that are conserved in ATP-grasp enzymes (Figure S2). This  
9  
10 observation makes a strong case for a common ancestry of Cdc123 and ATP-grasp enzymes.  
11  
12 However, significant differences are observed within their respective ATP binding sites. Such  
13  
14 divergences are likely to be linked to the biological function of Cdc123. Overall, Cdc123 may be  
15  
16 considered as an atypical member of the ATP-grasp family.  
17  
18

19 Notably, a second cavity faces the nucleotide-binding pocket in Cdc123 (Figure 3B). This  
20  
21 cavity is walled by residues V10, C13 and Q14 from  $\alpha 1$  on one side and by residues H134, D135 and  
22  
23 F140 from  $\alpha 6$  on the other side. In addition, the side chains of R246 and W99 are positioned at the top  
24  
25 and bottom of the cavity, respectively. In the ADP-bound structure, the cavity is filled up by electron  
26  
27 density attributed to five water molecules. According to the location of the second binding pocket and  
28  
29 to the homology with the ATP-grasp enzymes, it is conceivable that this pocket corresponds to a  
30  
31 binding site for a second ligand of Cdc123, substrate of a reaction involving an ATP-dependent  
32  
33 ligation step as observed in ATP-grasp enzymes. The existence of such an unidentified second ligand  
34  
35 remains however hypothetical at this stage.  
36  
37  
38  
39  
40  
41

#### 42 *Binding of Cdc123 to eIF2 $\gamma$*

43  
44  
45 *In vivo* assembly of the eIF2 complex was shown to depend on Cdc123. Sc-Cdc123 activity  
46  
47 involved an interaction with the unassembled eIF2 $\gamma$  subunit (Perzmaier et al., 2013). eIF2 $\gamma$  is made of  
48  
49 three domains: the GTP-binding domain,  $\gamma$ DI, and the two  $\beta$ -barrels  $\gamma$ DII and  $\gamma$ DIII (Schmitt et al.,  
50  
51 2010). Within eIF2 $\gamma$ , domain III was shown to be sufficient for binding to Cdc123 (Perzmaier et al.,  
52  
53 2013).  
54  
55

56 According to these results, we evidenced *in vitro* interaction of Sc-Cdc123 to Sc-eIF2 $\gamma$ DIII  
57  
58 domain (domain III of eIF2 $\gamma$  from *S. cerevisiae*) using molecular sieving experiments (Figure S3 and  
59  
60  
61

1 Experimental Procedures). Interestingly, the behavior of Sc-Cdc123 on the molecular sieve column  
2 suggested that the protein was dimeric in its unliganded form and became monomeric upon binding to  
3 eIF2 $\gamma$ DIII (Figure S3). The K<sub>d</sub> value for the binding of Sc-eIF2 $\gamma$ DIII to Sc-Cdc123 was 2.5  $\pm$  0.5  $\mu$ M,  
4 as measured using ITC (Figure S3). This value was measured in the absence of ATP. Hence, binding  
5 of Sc-eIF2 $\gamma$ DIII to Sc-Cdc123 did not strictly require the presence of ATP-Mg<sup>2+</sup>. Despite several  
6 attempts, no crystal could be obtained using the purified complex. Therefore, we decided to design a  
7 chimeric complex made of Sp-Cdc123 bound to Sc-eIF2 $\gamma$ DIII. Formation of a stable complex was  
8 indeed observed by a pull-down experiment showing that an N-terminally his-tagged version of Sp-  
9 Cdc123 can trap Sc-eIF2 $\gamma$ DIII on a cobalt affinity resin. Upon elution with imidazole, a peak  
10 corresponding to a heterodimer of Sp-Cdc123 bound to Sc-eIF2 $\gamma$ DIII was observed (Experimental  
11 Procedures). An additional step using molecular sieving allowed us to polish the purification (Figure  
12 S3). Notably, the binding of Sc-eIF2 $\gamma$ DIII to Sp-Cdc123 did not produce sufficient heat changes to  
13 allow accurate determination of a K<sub>d</sub> value using ITC. One possible explanation is that, in the case of  
14 the complex formed with the *S. cerevisiae* proteins, binding of Sc-Cdc123 to Sc-eIF2 $\gamma$ DIII is  
15 accompanied by a change of the oligomeric state of Sc-Cdc123 from homodimer to monomer. Sp-  
16 Cdc123 behaves as a monomer and binding to Sc- $\gamma$ DIII does not change its oligomeric state, possibly  
17 explaining why observed heat changes are weaker.

18  
19  
20  
21  
22  
23  
24  
25  
26  
27  
28  
29  
30  
31  
32  
33  
34  
35  
36  
37  
38  
39 Suitable crystals were obtained using the purified complex Sp-Cdc123:Sc-eIF2 $\gamma$ DIII at 24°C  
40 in the presence or in the absence of ATP-Mg<sup>2+</sup>. The structure was solved by molecular replacement  
41 using the structure of Sp-Cdc123 $\Delta$ c determined in this study and the structure of eIF2 $\gamma$ DIII from *S.*  
42 *solfataricus* (2AHO, (Yatime et al., 2006)) as search models. The structures were refined to 2.9 Å and  
43 3.0 Å resolution in the presence or in the absence of ATP-Mg<sup>2+</sup>, respectively (Table 1).

44  
45  
46  
47  
48  
49  
50  
51  
52  
53  
54  
55  
56  
57  
58  
59  
60  
61  
62  
63  
64  
65  
66  
67  
68  
69  
70  
71  
72  
73  
74  
75  
76  
77  
78  
79  
80  
81  
82  
83  
84  
85  
86  
87  
88  
89  
90  
91  
92  
93  
94  
95  
96  
97  
98  
99  
100  
101  
102  
103  
104  
105  
106  
107  
108  
109  
110  
111  
112  
113  
114  
115  
116  
117  
118  
119  
120  
121  
122  
123  
124  
125  
126  
127  
128  
129  
130  
131  
132  
133  
134  
135  
136  
137  
138  
139  
140  
141  
142  
143  
144  
145  
146  
147  
148  
149  
150  
151  
152  
153  
154  
155  
156  
157  
158  
159  
160  
161  
162  
163  
164  
165  
166  
167  
168  
169  
170  
171  
172  
173  
174  
175  
176  
177  
178  
179  
180  
181  
182  
183  
184  
185  
186  
187  
188  
189  
190  
191  
192  
193  
194  
195  
196  
197  
198  
199  
200  
201  
202  
203  
204  
205  
206  
207  
208  
209  
210  
211  
212  
213  
214  
215  
216  
217  
218  
219  
220  
221  
222  
223  
224  
225  
226  
227  
228  
229  
230  
231  
232  
233  
234  
235  
236  
237  
238  
239  
240  
241  
242  
243  
244  
245  
246  
247  
248  
249  
250  
251  
252  
253  
254  
255  
256  
257  
258  
259  
260  
261  
262  
263  
264  
265  
266  
267  
268  
269  
270  
271  
272  
273  
274  
275  
276  
277  
278  
279  
280  
281  
282  
283  
284  
285  
286  
287  
288  
289  
290  
291  
292  
293  
294  
295  
296  
297  
298  
299  
300  
301  
302  
303  
304  
305  
306  
307  
308  
309  
310  
311  
312  
313  
314  
315  
316  
317  
318  
319  
320  
321  
322  
323  
324  
325  
326  
327  
328  
329  
330  
331  
332  
333  
334  
335  
336  
337  
338  
339  
340  
341  
342  
343  
344  
345  
346  
347  
348  
349  
350  
351  
352  
353  
354  
355  
356  
357  
358  
359  
360  
361  
362  
363  
364  
365  
366  
367  
368  
369  
370  
371  
372  
373  
374  
375  
376  
377  
378  
379  
380  
381  
382  
383  
384  
385  
386  
387  
388  
389  
390  
391  
392  
393  
394  
395  
396  
397  
398  
399  
400  
401  
402  
403  
404  
405  
406  
407  
408  
409  
410  
411  
412  
413  
414  
415  
416  
417  
418  
419  
420  
421  
422  
423  
424  
425  
426  
427  
428  
429  
430  
431  
432  
433  
434  
435  
436  
437  
438  
439  
440  
441  
442  
443  
444  
445  
446  
447  
448  
449  
450  
451  
452  
453  
454  
455  
456  
457  
458  
459  
460  
461  
462  
463  
464  
465  
466  
467  
468  
469  
470  
471  
472  
473  
474  
475  
476  
477  
478  
479  
480  
481  
482  
483  
484  
485  
486  
487  
488  
489  
490  
491  
492  
493  
494  
495  
496  
497  
498  
499  
500  
501  
502  
503  
504  
505  
506  
507  
508  
509  
510  
511  
512  
513  
514  
515  
516  
517  
518  
519  
520  
521  
522  
523  
524  
525  
526  
527  
528  
529  
530  
531  
532  
533  
534  
535  
536  
537  
538  
539  
540  
541  
542  
543  
544  
545  
546  
547  
548  
549  
550  
551  
552  
553  
554  
555  
556  
557  
558  
559  
560  
561  
562  
563  
564  
565  
566  
567  
568  
569  
570  
571  
572  
573  
574  
575  
576  
577  
578  
579  
580  
581  
582  
583  
584  
585  
586  
587  
588  
589  
590  
591  
592  
593  
594  
595  
596  
597  
598  
599  
600  
601  
602  
603  
604  
605  
606  
607  
608  
609  
610  
611  
612  
613  
614  
615  
616  
617  
618  
619  
620  
621  
622  
623  
624  
625  
626  
627  
628  
629  
630  
631  
632  
633  
634  
635  
636  
637  
638  
639  
640  
641  
642  
643  
644  
645  
646  
647  
648  
649  
650  
651  
652  
653  
654  
655  
656  
657  
658  
659  
660  
661  
662  
663  
664  
665  
666  
667  
668  
669  
670  
671  
672  
673  
674  
675  
676  
677  
678  
679  
680  
681  
682  
683  
684  
685  
686  
687  
688  
689  
690  
691  
692  
693  
694  
695  
696  
697  
698  
699  
700  
701  
702  
703  
704  
705  
706  
707  
708  
709  
710  
711  
712  
713  
714  
715  
716  
717  
718  
719  
720  
721  
722  
723  
724  
725  
726  
727  
728  
729  
730  
731  
732  
733  
734  
735  
736  
737  
738  
739  
740  
741  
742  
743  
744  
745  
746  
747  
748  
749  
750  
751  
752  
753  
754  
755  
756  
757  
758  
759  
760  
761  
762  
763  
764  
765  
766  
767  
768  
769  
770  
771  
772  
773  
774  
775  
776  
777  
778  
779  
780  
781  
782  
783  
784  
785  
786  
787  
788  
789  
790  
791  
792  
793  
794  
795  
796  
797  
798  
799  
800  
801  
802  
803  
804  
805  
806  
807  
808  
809  
810  
811  
812  
813  
814  
815  
816  
817  
818  
819  
820  
821  
822  
823  
824  
825  
826  
827  
828  
829  
830  
831  
832  
833  
834  
835  
836  
837  
838  
839  
840  
841  
842  
843  
844  
845  
846  
847  
848  
849  
850  
851  
852  
853  
854  
855  
856  
857  
858  
859  
860  
861  
862  
863  
864  
865  
866  
867  
868  
869  
870  
871  
872  
873  
874  
875  
876  
877  
878  
879  
880  
881  
882  
883  
884  
885  
886  
887  
888  
889  
890  
891  
892  
893  
894  
895  
896  
897  
898  
899  
900  
901  
902  
903  
904  
905  
906  
907  
908  
909  
910  
911  
912  
913  
914  
915  
916  
917  
918  
919  
920  
921  
922  
923  
924  
925  
926  
927  
928  
929  
930  
931  
932  
933  
934  
935  
936  
937  
938  
939  
940  
941  
942  
943  
944  
945  
946  
947  
948  
949  
950  
951  
952  
953  
954  
955  
956  
957  
958  
959  
960  
961  
962  
963  
964  
965  
966  
967  
968  
969  
970  
971  
972  
973  
974  
975  
976  
977  
978  
979  
980  
981  
982  
983  
984  
985  
986  
987  
988  
989  
990  
991  
992  
993  
994  
995  
996  
997  
998  
999  
1000

1 domain of Sp-Cdc123 ( $\alpha$ 10, residues 297 to 315). Superimposition of the structure of the complex  
2 obtained in the presence of ATP on that obtained without ATP showed only adjustments of side chains  
3 involved in the binding of ATP.  
4  
5  
6  
7  
8

#### 9 *Overall structure of Sp-Cdc123:Sc-eIF2 $\gamma$ DIII*

10 Sc-eIF2 $\gamma$ DIII forms a  $\beta$ -barrel highly homologous to the corresponding domain in archaeal  
11 aIF2 (Figure S4). Two differences are notable. In the eukaryotic domain, (i) the loop between  $\beta$ 16 and  
12  $\beta$ 17 is longer and, (ii)  $\beta$ 21 is extended by four residues in such a way that its interaction with strand  
13  $\beta$ 16 is reinforced.  
14  
15  
16  
17  
18  
19  
20

21 In the structure of the complex, the  $\gamma$ DIII domain is bound to one side of Cdc123 domain 1.  
22 Neither Cdc123-domain 2 nor the C-terminal helix  $\alpha$ 10 does contact  $\gamma$ DIII (Figure 4A).  $\gamma$ DIII and  
23 Cdc123 closely interact together with an interaction surface of 1307 Å<sup>2</sup>. Interestingly, the binding site  
24 of  $\gamma$ DIII to Cdc123 overlaps the dimerization site of Cdc123 observed in all crystal forms. In order to  
25 address the possibility that the observed position of  $\gamma$ DIII to Cdc123 may have resulted from  
26 crystallization artifacts, a solution study was carried out using small angle X-ray scattering. The goal  
27 was to compare theoretical X-ray scattering curve deduced from the crystallographic structure with the  
28 scattering curve experimentally observed in solution. As shown in Figure 4B, the SAXS experimental  
29 curve obtained with the purified Sp-Cdc123:Sc-eIF2 $\gamma$ DIII fits very nicely the curve calculated from  
30 the crystal structure coordinates. This strongly argues in favor of the biological significance of our  
31 crystalline model.  
32  
33  
34  
35  
36  
37  
38  
39  
40  
41  
42  
43  
44  
45

46 Detailed interactions of Sp-Cdc123 with Sc-eIF2 $\gamma$ DIII are shown in Figure 4C and D. Sc-  
47 eIF2 $\gamma$ DIII is mainly bound through its concave side formed by strands  $\beta$ 17- $\beta$ 18- $\beta$ 19- $\beta$ 20- $\beta$ 21 of the  
48 barrel and by the  $\beta$ 20- $\beta$ 21 loop (Figure 4D). On the side of Cdc123, the main regions of contacts  
49 correspond to  $\alpha$ 3 and the following loop (residues 44, 46-50), helix  $\eta$ 2 (residues 107-110),  $\alpha$ 5 and  $\alpha$ 6  
50 (Figure 4C). Notably, the Cdc123 regions involved in the binding of Sc-eIF2 $\gamma$ DIII correspond to  
51 regions specific of Cdc123 proteins, not found in ATP-grasp enzymes (Figures 2 and S2, green  
52 regions). Figures S1, S4 and Table 2 show residues involved in the heterodimer interface between  
53  
54  
55  
56  
57  
58  
59  
60  
61  
62  
63  
64  
65

1 Cdc123 and  $\gamma$ DIII. Superimposition of bound Cdc123 on unbound Cdc123 showed that binding to  
2  $\gamma$ DIII involved adjustment of the interface regions. In particular,  $\alpha$ 3 and the following loop are  
3 displaced and the conformation of the region around helix  $\eta$ 2 (residues 107-110) is adjusted. This part  
4 of Cdc123 is connected to the ATP binding pocket (Figure 4C and D). Nevertheless, the  $K_d$  value of  
5 ATP measured by ITC for Sp-Cdc123:Sc-eIF2 $\gamma$ DIII ( $57 \pm 7 \mu\text{M}$ ) was not significantly changed as  
6 compared to that measured for isolated Sp-Cdc123 ( $67 \pm 13 \mu\text{M}$ ).  
7  
8  
9  
10  
11  
12

13 Previous results had suggested that within domain III, the C-terminal tail, specific of  
14 eukaryotic eIF2 $\gamma$  was required for the interaction with Cdc123. Indeed, removal of thirteen amino  
15 acids at the C-terminal extremity of eIF2 $\gamma$  (residues 515 to 527) was sufficient to render the protein  
16 non-functional in the binding to Cdc123 or to eIF2 $\alpha$  and eIF2 $\beta$  subunits (Perzmaier et al., 2013). On  
17 the contrary, the removal of 4 amino acids from the C-terminus was tolerated, since binding to Cdc123  
18 and assembly with  $\alpha$  and  $\gamma$  subunit still occurred (Perzmaier et al., 2013). No direct interaction is  
19 observed between the C-terminal part of  $\gamma$ DIII and Cdc123 in the structure of the complex. However,  
20 the structure shows that the last  $\beta$ -strand of  $\gamma$ DIII ( $\beta$ 21) is extended to residue 522. Therefore, it is  
21 likely that a deletion of residues belonging to  $\beta$ 21 led to destabilization of the structure of the  $\beta$ -barrel  
22 and thereby impaired binding to Cdc123. According to these observations, the absence of C-terminal  
23 extension in archaeal aIF2 $\gamma$ DIII cannot be straightforwardly related to the absence of Cdc123 from  
24 archaea.  
25  
26  
27  
28  
29  
30  
31  
32  
33  
34  
35  
36  
37  
38  
39  
40  
41

42 To further characterize the complex between Cdc123 and eIF2 $\gamma$ DIII, mutations within  $\gamma$ DIII  
43 were introduced. Three single mutants were produced, E460A, R504A and W509A. The effect of the  
44 mutations on association with Sp-Cdc123 was evaluated using pull-down assays (Figure S4). As  
45 predicted from the 3D structure, modification of R504 and W509 into alanine resulted in lower  
46 amount of Sp-Cdc123:Sc-eIF2 $\gamma$ DIII complex retained on affinity column, as compared to that  
47 obtained with wild-type Sc-eIF2 $\gamma$ DIII (Figure S4). In the case of E460A mutant, a lower level of  
48 protein expression did not allow us to reach a firm conclusion.  
49  
50  
51  
52  
53  
54  
55  
56  
57  
58  
59

60 *ATP binding residues of Cdc123 are crucial for eIF2 assembly*

1 Crystals of Sp-Cdc123:Sc-eIF2 $\gamma$ DIII complex could be obtained in the presence of ATP-Mg<sup>2+</sup>  
2 (Table 1). As shown in Figures 5 and S5A, ATP-Mg<sup>2+</sup> is observed, firmly bound to Cdc123 in the  
3 presence of one Mg<sup>2+</sup> ion. The octahedral coordination of the tightly bound magnesium ion is visible.  
4 In the equatorial plane, four bonds involve D239 and N241 side chains and two oxygens from the  
5  $\beta$  and  $\gamma$  phosphate groups. Two water molecules are in apical positions. One of them is stabilized by  
6 D227, whereas the second water appears less stable. Superimposition of Sp-Cdc123:Sc-  
7 eIF2 $\gamma$ DIII:ATP on Cdc123 $\Delta$ c:ADP shows that the two structures are nearly identical in the area of the  
8 nucleotide, with only adjustments of side chain residues involved in the binding of Mg<sup>2+</sup> and of the  $\gamma$   
9 phosphate group (Figure S5B).  
10  
11  
12  
13  
14  
15  
16  
17  
18  
19

20 Interestingly, in-line with the  $\gamma$ -phosphate of ATP is a water molecule located at 3.3 Å from  
21 the oxygens, at the entrance of the second cavity. This water molecule, stabilized by interactions with  
22 the main chain NH group of D248 and with the side chain NH<sub>2</sub> group of R176, would be correctly  
23 positioned to participate in a possible ATP hydrolysis reaction (Figure 5A and Figure S5B). At this  
24 moment, however, such an activity has not been firmly established.  
25  
26  
27  
28  
29  
30

31 To get further insight into the role of ATP in eIF2 assembly, mutants of Sc-Cdc123 were  
32 designed and their behaviors were studied *in vivo*.  
33  
34  
35

36 We targeted residues involved in the coordination of the ATP-bound Mg<sup>2+</sup> ion. Indeed, these  
37 residues (D227, D239, N241 in Sp-Cdc123) are highly conserved in Cdc123 sequences and in ATP-  
38 grasp enzymes (Figures S1 and S2). Moreover, various studies of ATP-grasp enzymes have shown  
39 that these residues are essential for the enzymatic activity and suggested that Mg<sup>2+</sup> had a catalytic role  
40 by maintaining ATP into a correct conformation for catalysis (Miller et al., 2005; Sloane et al., 2001).  
41 Therefore, we mutated the “DIN” sequence of Sc-Cdc123 (DIN; 266-268 in Sc-Cdc123 corresponding  
42 to 239-241 in Sp-Cdc123, Figure S1) into three alanines. To test the effect of the DIN mutation *in*  
43 *vivo*, we used diploid yeast cells heterozygote for a *CDC123* gene deletion, and expressing either wild  
44 type *CDC123* or the DIN mutant (Figure 5B, right panel). No complementation of a deletion of the  
45 *CDC123* gene was observed in the presence of the Sc-Cdc123 DIN. Moreover, the DIN mutant also  
46 failed to support assembly of Sc-eIF2 $\gamma$  with eIF2 $\alpha$  (Figure 5B, left panel). This observation was made  
47  
48  
49  
50  
51  
52  
53  
54  
55  
56  
57  
58  
59  
60  
61  
62  
63  
64  
65

1 in a *S. cerevisiae* strain deleted for *CDC123* and kept alive by high-level expression of eIF2 $\gamma$  and  
2 eIF2 $\alpha$ . Relative to a strain that carries the *CDC123* gene, there was much less eIF2 $\gamma$ -eIF2 $\alpha$  association  
3  
4 in the *cdc123* deletion mutant. Expression of the wild type version of Cdc123 restored normal eIF2 $\gamma$ -  
5  
6 eIF2 $\alpha$  association. Expression of the Sc-Cdc123 DIN mutant, however, failed to increase the  
7  
8 association of eIF2 $\gamma$  with eIF2 $\alpha$  (Figure 5B, left panel). Thus, ATP-binding residues are essential for  
9  
10 Cdc123 to support cell viability and eIF2 $\gamma$ -eIF2 $\alpha$  assembly. Using co-IP experiments, we observed a  
11  
12 defect of the DIN mutant in its interaction with full-length eIF2 $\gamma$ , whereas the amount of co-  
13  
14 precipitated eIF2 $\alpha$  was unaffected by the DIN mutation (Figure S6A). This points to a link between  
15  
16 ATP and the binding of full-length eIF2 $\gamma$  by Cdc123.  
17  
18  
19  
20

21 To substantiate these observations, we analyzed another mutant of the ATP binding site of  
22  
23 Cdc123, Sc-CDC123-D252A (equivalent to *S. pombe* D227) mutant. This residue, as D266 and N268,  
24  
25 participates in the binding of the magnesium ion through a water-mediated interaction (Table 3). In  
26  
27 line with the DIN mutant, Sc-CDC123-D252A failed to complement a *CDC123* gene deletion and did  
28  
29 not support assembly of eIF2 $\gamma$  with eIF2 $\alpha$  (Figure 5B). Together, these data show that the DIN and  
30  
31 D252A mutations disrupt both the biological and biochemical function of Cdc123. Hence, these  
32  
33 results strongly argue in favor of a requirement on ATP binding for the vital cellular function of  
34  
35 Cdc123 and for its role in promoting eIF2 $\alpha\gamma$  assembly.  
36  
37  
38  
39  
40

#### 41 *Model for the catalytic complex*

42  
43  
44 In order to go forward in understanding the mechanism used by Cdc123 for eIF2 assembly, we  
45  
46 performed a docking model for the binding of eIF2 $\gamma$  onto Cdc123. According to structural alignments  
47  
48 and biochemical data, the 3D structure of the eukaryotic  $\gamma$  subunit is supposed to be very close to that  
49  
50 of its archaeal counterpart (Schmitt et al., 2012). Therefore, to make the docking model, the Sc-  
51  
52 eIF2 $\gamma$ DIII domain from the Sp-Cdc123: $\gamma$ DIII structure, was superimposed on the corresponding  
53  
54 domain in aIF2 $\gamma$  structure (4RD4, (Dubiez et al., 2015)). In this model, shown in Figure 6A and B, the  
55  
56 complete eIF2 $\gamma$  subunit is nicely anchored to Cdc123, without intertwining. Interestingly, the docking  
57  
58 model revealed another potential contact between eIF2 $\gamma$  and Cdc123. This contact would involve the  
59  
60  
61  
62  
63  
64  
65

1 long L1 loop of eIF2 $\gamma$ -DII domain and the loop linking  $\beta$ 5 to  $\alpha$ 7 (residues 192-196) of Sp-Cdc123.

2 Strikingly, L1 loop of eIF2 $\gamma$ -DII domain is known to mediate interaction between eIF2 $\gamma$  and  
3 eIF2 $\alpha$  subunits (Naveau et al., 2013; Roll-Mecak et al., 2004; Schmitt et al., 2002; Yatime et al.,  
4 2006).  
5  
6

7  
8  
9 Importantly, the position of eIF2 $\gamma$  on Cdc123 is compatible with simultaneous binding to  
10 eIF2 $\alpha$ . Indeed, the docking model can be completed by positioning the eIF2 $\alpha$  subunit, thanks to the  
11 knowledge of the eIF2 $\alpha\gamma$  structure (PDB ID Code 2AHO, (Yatime et al., 2006)). As shown in Figure  
12 6C, the model suggests an interaction of Cdc123 with the interface between  $\alpha$  and  $\gamma$  subunits. Hence,  
13 the docking model opens the possibility that Cdc123 acts through transient interaction with the L1  
14 loop of  $\gamma$ DII and domain 3 of eIF2 $\alpha$  subunit. This interaction would be necessary for the assembly of  
15 eIF2 $\gamma$  and eIF2 $\alpha$ .  
16  
17  
18  
19  
20  
21  
22  
23  
24

25 To test the docking model, we generated a mutant version of eIF2 $\gamma$  lacking part of the L1 loop  
26 and analyzed its interaction with Sc-Cdc123 and the  $\alpha$  and  $\beta$  subunits in an Y2H assay. The L1 loop  
27 mutation had little or no effect on the interaction of eIF2 $\gamma$  with eIF2 $\beta$ , but disrupted the interaction of  
28 eIF2 $\gamma$  with eIF2 $\alpha$  and reduced the interaction of eIF2 $\gamma$  with Cdc123 (Figure S6B). The Y2H data,  
29 therefore, confirm the L1 loop region as an  $\alpha$ - $\gamma$  binding site in eukaryotic eIF2 orthologs and support  
30 the notion of a physical contact between the L1 loop of eIF2 $\gamma$  and Cdc123, as predicted by the docking  
31 model.  
32  
33  
34  
35  
36  
37  
38  
39  
40  
41

42 To further analyze the docking model, we asked for an interaction of Sc-Cdc123 with eIF2 $\alpha$ .  
43 To this end, we over-expressed a flag3-tagged version of Sc-Cdc123 in a yeast strain whose  
44 endogenous eIF2 $\alpha$ -encoding gene was fused to a myc13-tag. Indeed, eIF2 $\alpha$ -myc13 was detected in  
45 anti-flag immunoprecipitates of Cdc123. This signal was specific, because it was absent from  
46 precipitates of a control strain, which lacked Cdc123-flag3 but expressed eIF2 $\alpha$ -myc13 (Figure S6A).  
47  
48  
49  
50  
51  
52  
53  
54 This experiment demonstrates a contact between Cdc123 and eIF2 $\alpha$  or eIF2 $\alpha\gamma$ . Compared to the  
55 relative amount of eIF2 $\gamma$  co-precipitated with Cdc123-flag3 from cell extracts, much lower levels of  
56 eIF2 $\alpha$ -myc13 were recovered. The Cdc123- eIF2 $\alpha$  or -eIF2 $\alpha\gamma$  contact might therefore be transient.  
57  
58  
59  
60  
61  
62  
63  
64  
65

## DISCUSSION

The present study revealed the 3D structure of the cell proliferation protein Cdc123. This protein resembles enzymes belonging to the ATP-grasp superfamily. As suggested by this resemblance, ATP binding to Cdc123 could indeed be evidenced using biochemical tools and 3D structure determination. ATP is bound by residues common to Cdc123 and ATP-grasp enzymes but also by residues specific to Cdc123. Moreover, ATP-grasp enzymes possess an N-terminal domain, which makes part of their catalytic center. This domain is absent in Cdc123. Overall, Cdc123 protein appears as a member of the ATP-grasp family having unique features.

As in ATP-grasp enzymes, crucial residues are involved in the binding of the magnesium ion held on ATP. These residues (D252, D266, N268 in Sc-Cdc123 equivalent to D227, D239, N241 in Sp-Cdc123) were shown in this study to be essential for the cellular function of Cdc123. In the same view, it should be reminded that a temperature-sensitive mutant of a rat fibroblast line, arrested in the G1 phase of the cell cycle at restrictive temperature, was mapped within Cdc123 (Ohno et al., 1984; Okuda and Kimura, 1996). The mutation identified corresponds to a change of A109 into valine (equivalent to T101 in Sp-Cdc123). T101 indeed participates in the binding of ATP (Table 3). Therefore, this temperature-sensitive mutant gives further credit to the idea that ATP is needed for the cellular function of Cdc123.

Previous studies had shown that Cdc123 was necessary for eIF2 assembly (Perzmaier et al., 2013). In particular, interaction between unassembled eIF2 $\gamma$  and Cdc123 was evidenced, with DIII domain of eIF2 $\gamma$  being sufficient to trap Cdc123. Here, we determined the structure of Sp-Cdc123 bound to the  $\gamma$ DIII domain of eIF2. The  $\gamma$ DIII domain of eIF2 is bound to Cdc123 via interactions involving only Cdc123-domain 1. Domain 2 and the C-terminal domain do not contact  $\gamma$ DIII. This observation is consistent with results obtained using a yeast-2-hybrid assay and immunoprecipitation experiments, showing that C-terminal sequences of Sc-Cdc123 are dispensable for  $\gamma$  binding (Figure S6C). On the contrary, this C-terminal region is essential for Cdc123 function because cells carrying Cdc123 $\Delta$ 291 are inviable (Figure S6C). Consistently, association of the eIF2 subunits was

1  
2  
3  
4  
5  
6  
7  
8  
9  
10  
11  
12  
13  
14  
15  
16  
17  
18  
19  
20  
21  
22  
23  
24  
25  
26  
27  
28  
29  
30  
31  
32  
33  
34  
35  
36  
37  
38  
39  
40  
41  
42  
43  
44  
45  
46  
47  
48  
49  
50  
51  
52  
53  
54  
55  
56  
57  
58  
59  
60  
61  
62  
63  
64  
65

compromised when a truncated version of Sc-Cdc123 (Sc-Cdc123 $\Delta$ 327) was used (Perzmaier et al., 2013).

Accordingly, the docking model suggests that the C-terminal domain of Cdc123 is involved in the assembly process of eIF2 $\gamma$  to eIF2 $\alpha$ . Therefore, eIF2 $\gamma$  would be bound to Cdc123 by an anchoring point located in domain 1 of the Cdc123, as observed in the present Cdc123- $\gamma$ DIII structure. In this view, the Cdc123- $\gamma$ DIII structure might represent a “pre-assembly complex” (Figure 6). A second contact point, possibly dependent on ATP binding and/or ATP hydrolysis, involving domain 2 and the C-terminal domain of Cdc123 would be necessary for the reshaping of the interaction surface between eIF2 $\gamma$  and eIF2 $\alpha$ . Once assembled, the eIF2 $\alpha\gamma$  complex becomes stably folded allowing further spontaneous binding of the eIF2 $\beta$  subunit without the help of Cdc123 ((Perzmaier et al., 2013) and our unpublished observations). After assembly, Cdc123 no longer interacts with eIF2 (Perzmaier et al., 2013) even though the region of  $\gamma$ DIII involved in Cdc123 interface remains accessible (Figure 6C). This suggests that the release of Cdc123 might result from unfavourable interactions between the second contact point (domain 2 and C-terminal domain of Cdc123) and the reshaped eIF2 $\alpha\gamma$  association surface.

Notably, archaea do not display Cdc123 orthologs. Accordingly, assembly of aIF2 subunits occurs spontaneously *in vitro* (Pedulla et al., 2005; Stolboushkina et al., 2008; Yatime et al., 2006; Yatime et al., 2004). However, Sequence alignments highlighting the specificities of eukaryotic and archaeal e/aIF2 $\gamma$  do not give any obvious clue to explain the different behaviors of eIF2 and aIF2 regarding the assembly of the heterotrimer (Yatime et al., 2007).

Affecting ATP binding to Cdc123 led to the loss of Cdc123 function. Thus, our structural and biochemical data link the function of Cdc123 in eIF2 assembly to the cell energetics. This reinforces the idea that Cdc123 is an important control point of the eukaryotic cell cycle. The question of whether Cdc123 uses ATP in a chaperone-like fashion to support eIF2 $\alpha\gamma$  assembly without covalent modification or whether Cdc123 uses ATP to introduce a post-translational modification in an effector site remains open. The existence of a second binding pocket identified in the structure rather argues in favor of the second possibility. However, for the while, our attempts to evidence modification in

purified eIF2 $\gamma$  subunit from cells expressing or not Cdc123 have been fruitless. Therefore, further studies are clearly required to reveal how Cdc123 uses ATP to favor the assembly of eIF2.

1  
2  
3  
4  
5  
6  
7  
8  
9  
10  
11  
12  
13  
14  
15  
16  
17  
18  
19  
20  
21  
22  
23  
24  
25  
26  
27  
28  
29  
30  
31  
32  
33  
34  
35  
36  
37  
38  
39  
40  
41  
42  
43  
44  
45  
46  
47  
48  
49  
50  
51  
52  
53  
54  
55  
56  
57  
58  
59  
60  
61  
62  
63  
64  
65

## EXPERIMENTAL PROCEDURES

### Protein expression and purification

#### *Sp-Cdc123*

The gene coding for Sp-Cdc123 was amplified from a cDNA library (generous gift from François Lacroute, INRA, Grignon, France) and cloned into pET3a and pET15b derivatives. The resulting plasmids called pET3a-SpCdc123 and pET15b-SpCdc123 led to the expression of an untagged and an N-terminally tagged version of Sp-Cdc123, respectively. To express the protein, the desired plasmid was transformed into *E. coli* BL21 Rosetta pLacI-Rare (Merck, Novagen). 1 L cultures were in 2xTY containing 50 µg/mL of ampicillin and 34 µg/mL of chloramphenicol. Expression was induced by adding 1 mM of IPTG in an overnight 37°C culture. After induction, the cultures were continued for 5 hours at 18°C.

For untagged Sp-Cdc123, cells corresponding to 1 L of culture were disrupted by sonication in 30 mL of buffer A (10 mM HEPES pH 7.5, 200 mM NaCl, 3 mM 2-mercaptoethanol, 0.1 mM PMSF, 0.1 mM benzamidine). The crude extract was loaded onto a Q-Sepharose column (16 mm x 20 cm; GE-Healthcare) equilibrated in buffer A. A gradient from 200 mM NaCl to 1 M NaCl was used for elution (200 mL at a flow rate of 2.5 mL/min). This step was repeated twice. The recovered protein was loaded onto a Superdex 200 10/300 (GE-Healthcare) equilibrated in buffer A. The Sp-Cdc123 pool was concentrated to 10 mg/mL. Sp-Cdc123 behaves as a monomer in solution, as shown by conventional size-exclusion chromatography coupled to multi-angle static light scattering (SEC-MALS, Wyatt).

A truncated version of Sp-Cdc123 was engineered by introducing a stop codon in place of codon 275. The obtained plasmid, pET15b-SpCdc123Δc produced a protein ending at residue 274 and carrying a poly histidine tag at the N-terminal extremity. pET15b-SpCdc123Δc was transformed into *E. coli* BL21 Rosetta and expression was obtained as described above. After sonication, the crude extract was loaded onto a column (4 mL) containing Talon affinity resin (Clontech) equilibrated in buffer B (10 mM HEPES pH 7.5, 500 mM NaCl, 3 mM 2-mercaptoethanol, 0.1 mM PMSF, 0.1 mM benzamidine). The protein was eluted with buffer B containing 125 mM imidazole. The recovered

1 protein was then loaded onto a Superdex 200 column (10/300; GE Healthcare) equilibrated in buffer  
2 B. The Sp-Cdc123Δc pool was concentrated to 10 mg/mL.  
3

#### 4 5 6 *Sp-Cdc123:Sc-γDIII complex* 7

8  
9 The gene coding for the γDIII domain (fragment 410-527) of Sc-eIF2 from PWS3915  
10 (Perzmaier et al., 2013) was cloned in pET3alpa. The obtained plasmid pET3a-Sc-γDIII was  
11 transformed into *E. coli* BL21 Rosetta and expression was obtained as described above.  
12  
13

14  
15 To purify the Sp-Cdc123:Sc-γDIII complex, pellets corresponding to 1 liter of culture of BL21  
16 Rosetta *E. coli* cells transformed with pET3a-Sc-γDIII and to 1 liter of culture of BL21 rosetta *E. coli*  
17 cells transformed with pET15b-Sp-Cdc123 were resuspended in buffer B (10 mM HEPES pH 7.5, 500  
18 mM NaCl, 3 mM 2-mercaptoethanol, 0.1 mM PMSF, 0.1 mM benzamidine) and mixed. After  
19 sonication, the crude extract was loaded onto a column (4 mL) containing Talon affinity resin  
20 (Clontech) equilibrated in buffer B. Finally, the protein complex was eluted with buffer B containing  
21 125 mM imidazole. The recovered protein complex was finally loaded onto a Superdex 200 column  
22 (10/300; GE Healthcare) equilibrated in buffer B. Fractions containing Sp-Cdc123:Sc-γDIII were  
23 pooled and concentrated to 10 mg/mL (Figure S3B).  
24  
25  
26  
27  
28  
29  
30  
31  
32  
33  
34  
35  
36  
37  
38

#### 39 **Crystallization and structure determinations**

##### 40 *Sp-Cdc123* 41

42  
43 Initial crystallization trials were performed at 4°C and 24°C using sitting drops made with a  
44 Mosquito robot (TTP Labtech) and standard commercial kits (Hampton Research and Qiagen).  
45 Crystals were rapidly obtained using full-length Cdc123 in the presence of PEG3350 as precipitating  
46 agent at 24°C (see detailed conditions in Table S1). Diffraction data were collected at 100 K ( $\lambda=0.984$   
47 Å) on the Proxima-1 beamline at the SOLEIL synchrotron (Saint-Aubin, FRANCE) equipped with a  
48 Pilatus detector. Data corresponding to crystals belonging to various space groups were collected  
49 (Table S1). These crystals diffracted to a maximum of 3.0 Å resolution. Diffraction images were  
50  
51  
52  
53  
54  
55  
56  
57  
58  
59  
60  
61  
62  
63  
64  
65

1 analyzed with XDS (Kabsch, 1988), and the data were processed with programs of the CCP4 package  
2 (Collaborative computational project No.4, 1994).  
3

4 Crystals were also obtained using the selenomethionylated version of full-length Cdc123.  
5  
6 Highly redundant anomalous datasets were collected at 100K at a wavelength corresponding to the  
7 maximal absorption of selenium ( $\lambda=0.9792 \text{ \AA}$ ). According to the weak diffraction pattern and to the  
8 modest resolution limit of diffraction (around  $4 \text{ \AA}$ ), two datasets collected from Se-met crystals grown  
9 in the same drop, were merged. A first experimental map was calculated at  $5.5 \text{ \AA}$  resolution using the  
10 automated SAD phasing procedure of the Solve program within the Phenix suite (Adams et al., 2010).  
11  
12 A first round of automatic building was performed within this map using the “Phase and Build”  
13 function in Solve. The partial model allowed determination of the non-crystallographic symmetry  
14 operators. In a second step, a dataset corresponding to a crystal of full-length Cdc123 obtained in  
15 space group  $P2_12_12_1$  was used to perform multiple crystal averaging (Table S1). The quality of the  
16 resulting map was clearly improved and allowed manual building of a first model in Coot (Emsley et  
17 al., 2010). During manual building, the Dali Server was used to search for possible homologous  
18 structures. The crystal structure of the D-alanine--D-Alanine Ligase from *Bacillus anthracis*  
19 complexed with ATP (PDB ID code 3R5X) was identified and then used as a guide to facilitate further  
20 model building. In the course of refinement, the dataset corresponding to a crystal belonging to space  
21 group C222 was finally used to complete building of the model (Table S1). The preliminary structure  
22 of Cdc123 was partially refined to  $3.24 \text{ \AA}$  resolution ( $R=0.2689$ ,  $R_{\text{free}}=0.3079$ ). This first model  
23 revealed that full-length Cdc123 was only partly defined in the electron density with residues 274 to  
24 319 being not visible. Therefore, in order to improve the quality of the crystals, a C-terminally  
25 truncated form of Cdc123 was then engineered. Crystals obtained with the C-terminally truncated  
26 form of Cdc123 (Sp-Cdc123 $\Delta$ c) diffracted to  $1.85 \text{ \AA}$  resolution (see detailed conditions in Table 1).  
27  
28 New datasets were collected in the presence or in the absence of ATP or ATP analogs (Table 1). The  
29  $3.24 \text{ \AA}$  resolution model was used to solve the structures by molecular replacement using Phaser. The  
30 final structures of Cdc123 $\Delta$ c were refined to  $1.85 \text{ \AA}$  and  $2.06 \text{ \AA}$  resolution, in the presence or in the  
31 absence of ADP, respectively, using standard procedures in Phenix. Final statistics are shown in Table  
32  
33  
34  
35  
36  
37  
38  
39  
40  
41  
42  
43  
44  
45  
46  
47  
48  
49  
50  
51  
52  
53  
54  
55  
56  
57  
58  
59  
60  
61  
62  
63  
64  
65

1  
2 *Sp-Cdc123:Sc-eIF2 $\gamma$ DIII* complex  
3

4 The complex stored in buffer B was used for crystallization trials. Crystals were obtained in  
5  
6 the presence of 25% PEG3350 and 0.2 M LiSO<sub>4</sub> with or without ATP-Mg<sup>2+</sup> (see detailed conditions in  
7  
8 Table 1). Datasets were collected on the PX1 beamline at the SOLEIL synchrotron (Saint-Aubin,  
9  
10 FRANCE). The same procedure as the one described above was used to process the data. The structure  
11  
12 was solved by molecular replacement with Phaser (Storoni et al., 2004), using the Cdc123 $\Delta$ c structure  
13  
14 determined in this work and the  $\gamma$ DIII domain from archaeal aIF2 $\gamma$  (PDB ID code 2AHO) as search  
15  
16 models. The final structures were refined to 2.9 Å and 3.0 Å resolution in the presence or in the  
17  
18 absence of ATP-Mg<sup>2+</sup>, respectively (Table 1). According to the relatively modest resolution of the  
19  
20 dataset as well as to the high B value of the structure, attribution of the sequence in the disconnected  
21  
22 helix 275-296 remained tentative.  
23  
24  
25  
26  
27  
28

29 **Accession numbers**  
30

31 Structure coordinates, 4ZGO (Sp-Cdc123 $\Delta$ c), 4ZGP(Sp-Cdc123 $\Delta$ c:ADP), 4ZGN (Sp-  
32  
33 Cdc123:Sc- $\gamma$ DIII:ATP), 4ZGQ (Sp-Cdc123:Sc- $\gamma$ DIII) have been deposited to the PDB.  
34  
35  
36  
37  
38  
39  
40  
41  
42  
43  
44  
45  
46  
47  
48  
49  
50  
51  
52  
53  
54  
55  
56  
57  
58  
59  
60  
61  
62  
63  
64  
65

1  
2 **AUTHOR CONTRIBUTIONS**  
3

4 ES, WS, YM designed research. MP, ED, LA, JP, ES, YM performed the experiments. ES,  
5  
6 WS, YM wrote the paper and all authors revised the manuscript.  
7  
8  
9

10  
11 **ACKNOWLEDGEMENTS**  
12

13 This work was supported by grants from the Centre National de la Recherche Scientifique and  
14  
15 by Ecole polytechnique to Unité Mixte de Recherche n°7654. ED was a recipient of a Gaspard Monge  
16  
17 PhD fellowship from Ecole polytechnique. We thank the staff of the macromolecular crystallography  
18  
19 beamlines at the SOLEIL synchrotron (Saclay, France) and in particular Pierre Legrand, for expert  
20  
21 assistance during data collection and Andrea Brücher, Antje Machetanz-Morokane, and Adelheid  
22  
23 Weissgerber for their expert technical assistance with the yeast work. We thank François Lacroute  
24  
25 (Institut National de la Recherche Agronomique, Grignon, France) for generous gift of the *S. pombe*  
26  
27 cDNA library.  
28  
29  
30  
31  
32

33 **REFERENCES**  
34

35 Adams, P.D., Afonine, P.V., Bunkóczi, G., Chen, V.B., Davis, I.W., Echols, N., Headd, J.J., Hung, L.-  
36 W., Kapral, G.J., Grosse-Kunstleve, R.W., *et al.* (2010). PHENIX: a comprehensive Python-based  
37 system for macromolecular structure solution. *Acta Cryst D66*, 213-221.  
38 Adelaide, J., Finetti, P., Bekhouche, I., Repellini, L., Geneix, J., Sircoulomb, F., Charafe-Jauffret, E.,  
39 Cervera, N., Desplans, J., Parzy, D., *et al.* (2007). Integrated profiling of basal and luminal breast  
40 cancers. *Cancer research* 67, 11565-11575.  
41 Algire, M.A., Maag, D., and Lorsch, J.R. (2005). Pi release from eIF2, not GTP hydrolysis, is the step  
42 controlled by start-site selection during eukaryotic translation initiation. *Mol Cell* 20, 251-262.  
43 Artymiuk, P.J., Poirrette, A.R., Rice, D.W., and Willett, P. (1996). Biotin carboxylase comes into the  
44 fold. *Nat Struct Biol* 3, 128-132.  
45 Cole, C., Barber, J., and Barton, G. (2008). The Jpred 3 secondary structure prediction server. *Nucleic  
46 Acids Research* 35 (suppl.2), W197-W201.  
47 Collaborative computational project No.4 (1994). The CCP4 suite: programs from protein  
48 crystallography. *Acta Crystallogr D50*, 760-763.  
49 Dubiez, E., Aleksandrov, A., Lazennec-Schurdevin, C., Mechulam, Y., and Schmitt, E. (2015).  
50 Identification of a second GTP-bound magnesium ion in archaeal initiation factor 2. *Nucleic Acids  
51 Res* 43, 2946-2957.  
52 Emsley, P., Lohkamp, B., Scott, W.G., and Cowtan, K. (2010). Features and development of Coot.  
53 *Acta Crystallogr D66*, 486-501.  
54 Fan, C., Moews, P.C., Shi, Y., Walsh, C.T., and Knox, J.R. (1995). A common fold for peptide  
55 synthetases cleaving ATP to ADP: glutathione synthetase and D-alanine:d-alanine ligase of  
56 *Escherichia coli*. *Proc Natl Acad Sci U S A* 92, 1172-1176.  
57  
58  
59  
60  
61  
62  
63  
64  
65

1 Fawaz, M.V., Topper, M.E., and Firestone, S.M. (2011). The ATP-grasp enzymes. *Bioorg Chem* 39,  
185-191.

2 Galperin, M.Y., and Koonin, E.V. (1997). A diverse superfamily of enzymes with ATP-dependent  
3 carboxylate-amine/thiol ligase activity. *Protein Sci* 6, 2639-2643.

4 Gebauer, F., and Hentze, M.W. (2004). Molecular mechanisms of translational control. *Nat Rev Mol*  
5 *Cell Biol* 5, 827-835.

6 Hara, T., Kato, H., Katsube, Y., and Oda, J. (1996). A pseudo-michaelis quaternary complex in the  
7 reverse reaction of a ligase: structure of *Escherichia coli* B glutathione synthetase complexed with  
8 ADP, glutathione, and sulfate at 2.0 Å resolution. *Biochemistry* 35, 11967-11974.

9 Hinnebusch, A.G. (2005). Translational regulation of GCN4 and the general amino acid control of  
10 yeast. *Annual review of microbiology* 59, 407-450.

11 Hinnebusch, A.G. (2011). Molecular mechanism of scanning and start codon selection in eukaryotes.  
12 *Microbiol Mol Biol Rev* 75, 434-467.

13 Ho, Y., Gruhler, A., Heilbut, A., Bader, G.D., Moore, L., Adams, S.L., Millar, A., Taylor, P., Bennett,  
14 K., Boutilier, K., *et al.* (2002). Systematic identification of protein complexes in *Saccharomyces*  
15 *cerevisiae* by mass spectrometry. *Nature* 415, 180-183.

16 Holcik, M., and Sonenberg, N. (2005). Translational control in stress and apoptosis. *Nat Rev Mol Cell*  
17 *Biol* 6, 318-327.

18 Holm, L., and Sander, C. (1995). Dali: a network tool for protein structure comparison. *Trends*  
19 *Biochem Sci* 20, 478-480.

20 Huang, H.K., Yoon, H., Hannig, E.M., and Donahue, T.F. (1997). GTP hydrolysis controls stringent  
21 selection of the AUG start codon during translation initiation in *Saccharomyces cerevisiae*. *Genes Dev*  
22 11, 2396-2413.

23 Kabsch, W.J. (1988). Evaluation of single crystal X-ray diffraction data from a position sensitive  
24 detector. *J Appl Crystallogr* 21, 916-924.

25 Laskowski, R.A., Mac Arthur, M.W., Moss, D.S., and Thornton, J.M. (1993). PROCHECK: a  
26 program to check the stereochemical quality of protein structure. *J Appl Crystallogr* 26, 283-291.

27 Liu, S., Chang, J.S., Herberg, J.T., Horng, M.M., Tomich, P.K., Lin, A.H. and Marotti, K.R. (2006).  
28 Allosteric inhibition of *Staphylococcus aureus* D-alanine:D-alanine ligase revealed by crystallographic  
29 studies. *Proc Natl Acad Sci U S A* 103, 15178-15183.

30 Lorsch, J., and Dever, T. (2010). Molecular view of 43S complex formation and start site selection in  
31 eukaryotic translation initiation. *J Biol Chem* 285, 21203-21207.

32 Miller, G.J., Wilson, M.P., Majerus, P.W., and Hurley, J.H. (2005). Specificity determinants in  
33 inositol polyphosphate synthesis: crystal structure of inositol 1,3,4-trisphosphate 5/6-kinase. *Mol Cell*  
34 18, 201-212.

35 Naveau, M., Lazennec-Schurdevin, C., Panvert, M., Dubiez, E., Mechulam, Y., and Schmitt, E.  
36 (2013). Roles of yeast eIF2alpha and eIF2beta subunits in the binding of the initiator methionyl-tRNA.  
37 *Nucleic Acids Res* 41, 1047-1057.

38 Ohno, K., Okuda, A., Ohtsu, M., and Kimura, G. (1984). Genetic analysis of control of proliferation in  
39 fibroblastic cells in culture. I. Isolation and characterization of mutants temperature-sensitive for  
40 proliferation or survival of untransformed diploid rat cell line 3Y1. *Somatic cell and molecular*  
41 *genetics* 10, 17-28.

42 Okuda, A., and Kimura, G. (1996). An amino acid change in novel protein D123 is responsible for  
43 temperature-sensitive G1-phase arrest in a mutant of rat fibroblast line 3Y1. *Experimental cell*  
44 *research* 223, 242-249.

45 Pedulla, N., Palermo, R., Hasenohrl, D., Blasi, U., Cammarano, P., and Londei, P. (2005). The  
46 archaeal eIF2 homologue: functional properties of an ancient translation initiation factor. *Nucleic*  
47 *Acids Res* 33, 1804-1812. Print 2005.

48 Perzmaier, A.F., Richter, F., and Seufert, W. (2013). Translation initiation requires cell division cycle  
49 123 (Cdc123) to facilitate biogenesis of the eukaryotic initiation factor 2 (eIF2). *J Biol Chem* 288,  
50 21537-21546.

51 Roll-Mecak, A., Alone, P., Cao, C., Dever, T.E., and Burley, S.K. (2004). X-ray structure of  
52 translation initiation factor eIF2gamma : implications for tRNA and eIF2alpha binding. *J Biol Chem*  
53 279, 10634-10642.

1 Roper, D.I., Huyton, T., Vagin, A., and Dodson, G. (2000). The molecular basis of vancomycin  
2 resistance in clinically relevant Enterococci: crystal structure of D-alanyl-D-lactate ligase (VanA).  
3 Proc Natl Acad Sci U S A 97, 8921-8925.  
4 Schmitt, E., Blanquet, S., and Mechulam, Y. (2002). The large subunit of initiation factor aIF2 is a  
5 close structural homologue of elongation factors. EMBO J 21, 1821-1832.  
6 Schmitt, E., Naveau, M., and Mechulam, Y. (2010). Eukaryotic and archaeal translation initiation  
7 factor 2: a heterotrimeric tRNA carrier. FEBS Lett 584, 405-412.  
8 Schmitt, E., Panvert, M., Lazennec-Schurdevin, C., Coureux, P.D., Perez, J., Thompson, A., and  
9 Mechulam, Y. (2012). Structure of the ternary initiation complex aIF2-GDPNP-methionylated initiator  
10 tRNA. Nat Struct Mol Biol 19, 450-454.  
11 Schrodinger, LLC (2010). The PyMOL Molecular Graphics System, Version 1.3r1.  
12 Sloane, V., Blanchard, C.Z., Guillot, F., and Waldrop, G.L. (2001). Site-directed mutagenesis of ATP  
13 binding residues of biotin carboxylase. Insight into the mechanism of catalysis. J Biol Chem 276,  
14 24991-24996.  
15 Soler Artigas, M., Loth, D.W., Wain, L.V., Gharib, S.A., Obeidat, M., Tang, W., Zhai, G., Zhao, J.H.,  
16 Smith, A.V., Huffman, J.E., *et al.* (2011). Genome-wide association and large-scale follow up  
17 identifies 16 new loci influencing lung function. Nat Genet 43, 1082-1090.  
18 Stolboushkina, E., Nikonov, S., Nikulin, A., Blasi, U., Manstein, D.J., Fedorov, R., Garber, M., and  
19 Nikonov, O. (2008). Crystal structure of the intact archaeal translation initiation factor 2 demonstrates  
20 very high conformational flexibility in the alpha- and beta-subunits. J Mol Biol 382, 680-691.  
21 Storoni, L.C., McCoy, A.J., and Read, R.J. (2004). Likelihood-enhanced fast rotation functions. Acta  
22 Crystallogr D60, 432-438.  
23 Yatime, L., Mechulam, Y., Blanquet, S., and Schmitt, E. (2006). Structural switch of the gamma  
24 subunit in an archaeal aIF2 alpha gamma heterodimer. Structure 14, 119-128.  
25 Yatime, L., Mechulam, Y., Blanquet, S., and Schmitt, E. (2007). Structure of an archaeal  
26 heterotrimeric initiation factor 2 reveals a nucleotide state between the GTP and the GDP states. Proc  
27 Natl Acad Sci U S A 104, 18445-18450.  
28 Yatime, L., Schmitt, E., Blanquet, S., and Mechulam, Y. (2004). Functional molecular mapping of  
29 archaeal translation initiation factor 2. J Biol Chem 279, 15984-15993.  
30 Zeggini, E., Scott, L.J., Saxena, R., Voight, B.F., Marchini, J.L., Hu, T., de Bakker, P.I., Abecasis,  
31 G.R., Almgren, P., Andersen, G., *et al.* (2008). Meta-analysis of genome-wide association data and  
32 large-scale replication identifies additional susceptibility loci for type 2 diabetes. Nat Genet 40, 638-  
33 645.  
34 Zhao, G., Jin, Z., Wang, Y., Allewell, N.M., Tuchman, M., and Shi, D. (2013). Structure and function  
35 of Escherichia coli RimK, an ATP-grasp fold, L-glutamyl ligase enzyme. Proteins 81, 1847-1854.  
36  
37  
38  
39  
40  
41  
42  
43  
44  
45  
46  
47  
48  
49  
50  
51  
52  
53  
54  
55  
56  
57  
58  
59  
60  
61  
62  
63  
64  
65

## FIGURE LEGENDS

### Figure 1: Structure of Sp-Cdc123

A-Schematic representation of the topology of Sp-Cdc123 $\Delta$ c. The  $\beta$ -strands are represented as arrows and the helices as rods. Secondary structure elements were assigned with PROCHECK (Laskowski et al., 1993). Domain 1 is colored in blue (residues 1-170) and domain 2 is colored in yellow (residues 171-274).

B-Cartoon representation of Sp-Cdc123 $\Delta$ c. Same color code as in view A. ADP is shown as sticks. Secondary structure elements are labeled. All structural views are drawn with PyMol (Schrodinger, 2010).

See also Figure S1.

### Figure 2: Comparison of sp-Cdc123 with D-alanyl-D-lactate ligase from ATP-grasp superfamily

A-Left: cartoon representation of Sp-Cdc123 $\Delta$ c. Domain 1 is colored in blue and domain 2 is colored in yellow except for regions specific to Cdc123 proteins which are colored in green. ATP is shown in sticks. Right: cartoon representation of (VanA) from *Enterococcus faecium* (PDB ID Code 1E4E, (Roper et al., 2000)). For the sake of clarity, the N-terminal domain is not represented. Parts of the central domain of 1E4E similar to Cdc123 are colored in blue, parts of the C-domain of 1E4E similar to Cdc123 are colored in yellow. Divergent regions as compared to Cdc123 are shown in green. The small and large loops overhanging ATP are shown in orange. ATP and a phosphorylated inhibitor bound to VanA are shown in sticks and spheres. The Magnesium ion is shown as a green sphere.

B-Left: Close-up view of the domain 1 of Sp-Cdc123 showing the three stranded  $\beta$ -sheet. Right: Close-up view of the central domain of 1E4E showing the four-stranded  $\beta$ -sheet and the two loops surrounding ATP. The color code is the same as in panel A. This view highlights the differences within the ATP-binding site between Cdc123 and the representative from the ATP-grasp family.

See also Figure S2.

1 C-Superimposition of the ATP-grasp core domain of Cdc123 (in blue and yellow, as in view A) onto  
2 the corresponding one in 1E4E (in grey). For the sake of clarity, divergent regions have been omitted.  
3  
4  
5

### 6 **Figure 3: Binding of ADP to Sp-Cdc123 $\Delta$ c**

7  
8 A-The residues involved in ADP binding and the corresponding electrostatic bonds are shown. Color  
9 code is the same as in Figure 2A. Water molecules are in red spheres.  
10

11  
12 B-Molecular surface representation of Sp-Cdc123 $\Delta$ c. Color code is the same as in Figure 2A. The  
13 view highlights the second cavity facing the ATP binding pocket.  
14  
15

16  
17 See also Figure S3.  
18  
19  
20  
21

### 22 **Figure 4: Structure of Sp-Cdc123:Sc-eIF2 $\gamma$ DIII complex**

23  
24 A-Overall structure of Sp-Cdc123:Sc- eIF2 $\gamma$ DIII complex. Sp-Cdc123 is colored as in Figure 1B. ATP  
25 is shown with sticks and Mg<sup>2+</sup> with a green sphere. Sc- $\gamma$ DIII is shown in orange.  
26  
27

28  
29 B-Solution studies using SAXS. The experimental SAXS curve (blue) is compared with the theoretical  
30 diffusion curve deduced from the crystalline structure of Sp-Cdc123:Sc- $\gamma$ DIII complex (red).  
31  
32

33  
34 C-Close-up view of Sp-Cdc123:Sc- $\gamma$ DIII showing the proximity of the ATP-binding pocket with the  
35 interface between the two proteins.  
36  
37

38  
39 D-Detailed interactions between Sp-Cdc123 and Sc- $\gamma$ DIII. The residues involved in the stabilization of  
40 the interface between the two proteins and the corresponding electrostatic interactions are shown (see  
41 also Table 2). The right view is rotated by 180° as compared to the left view.  
42  
43  
44

45  
46 See also Figure S4.  
47  
48  
49

### 50 **Figure 5: Binding of ATP-Mg<sup>2+</sup> to Sp-Cdc123:Sc- $\gamma$ DIII complex**

51  
52 A-The residues involved in ATP binding and the corresponding electrostatic interactions are shown.  
53

54  
55 Color code is the same as in Figure 3A. Water molecules are in red spheres and the magnesium ion in  
56 green sphere.  
57  
58  
59  
60  
61  
62  
63  
64  
65

1 B- Right panel: Failure of Cdc123-DIN (DIN266-268AAA) and Cdc123 D252A to support cell  
2 viability. Diploid yeast cells heterozygote for a *CDC123* gene deletion and expressing either a wild  
3 type copy of *CDC123* (upper panel; W14145), DIN (DIN266-268AAA; middle panel; W13936) or  
4 D252A (lower panel; W13935) mutant versions of *CDC123* were sporulated and subjected to tetrad  
5 dissection. Left panel: Failure of Cdc123-DIN (DIN266-268AAA) and Cdc123 D252A to support  
6 interaction of eIF2 $\gamma$  with eIF2 $\alpha$ . In yeast strains that overexpress a flag-tagged version of eIF2 $\gamma$   
7 /Gcd11 and eIF2 $\alpha$  /Sui2 and that carry either the endogenous wild type copy of *CDC123* (W7743;  
8 lane 1) or are deleted for *CDC123* (*cdc123-Δ*; lanes 2-5; W7745 lane 2) and express a wild type copy  
9 (W13930; lane 3), the DIN mutant version of *CDC123* (W13931; lane 4) or D252A (W14238; lane 5).  
10 Cdc123, eIF2 $\gamma$  and eIF2 $\alpha$  were detected by Western analysis of whole cell extracts (WCE). Flag-  
11 tagged eIF2 $\gamma$  was immunoprecipitated (IP) and precipitates were analyzed for the presence of eIF2 $\alpha$   
12 (Co-IP). Flag-eIF2 $\gamma$  was precipitated and detected with the monoclonal flag antibody M2. Cdc123 and  
13 eIF2 $\alpha$  were detected by rabbit antisera.

14 See also Figure S5.

### 15 **Figure 6: Model for the binding of Cdc123 to eIF2 $\alpha$**

16 A-Molecular surface representation of Sc-Cdc123: Sc-eIF2 $\gamma$ DIII complex. Color code is the same as  
17 that used in Figure 4.

18 B-Docking of aIF2 $\gamma$  onto Sp-Cdc123.

19 Sc-eIF2 $\gamma$ DIII domain from the Sp-Cdc123: $\gamma$ DIII structure, was superimposed on the corresponding  
20 domain in aIF2 $\gamma$  structure (4RD4, Dubiez et al., 2015). Sp-Cdc123: $\gamma$ DIII is colored as in view A.  
21 Domain I of aIF2 $\gamma$  is colored in green, domain II of aIF2 $\gamma$  is colored in red. An arrow indicates the  
22 long L1 loop responsible for the binding of aIF2 $\gamma$  to aIF2 $\alpha$  (Yatime et al., 2006).

23 C-Docking of aIF2 $\alpha$  onto Sp-Cdc123.

24 Sc-eIF2 $\gamma$ DIII domain from the Sp-Cdc123: $\gamma$ DIII structure, was superimposed on the corresponding  
25 domain in aIF2 $\alpha$  structure (see text, 2AHO, (Yatime et al., 2006)). Color code is the same as in view  
26

1 B for aIF2 $\gamma$  and Cdc123. aIF2 $\alpha$  is colored as follows: Domain 1 in dark blue, domain 2 in light blue  
2 and domain 3 in cyan.  
3

4 On the right of the structural views are schematics illustrating domain contacts within models of  
5 Cdc123:eIF2 $\gamma$  and Cdc123:eIF2 $\alpha\gamma$  complexes.  
6  
7

8  
9 See also Figure S6.  
10  
11  
12  
13  
14  
15  
16  
17  
18  
19  
20  
21  
22  
23  
24  
25  
26  
27  
28  
29  
30  
31  
32  
33  
34  
35  
36  
37  
38  
39  
40  
41  
42  
43  
44  
45  
46  
47  
48  
49  
50  
51  
52  
53  
54  
55  
56  
57  
58  
59  
60  
61  
62  
63  
64  
65

Figure 1

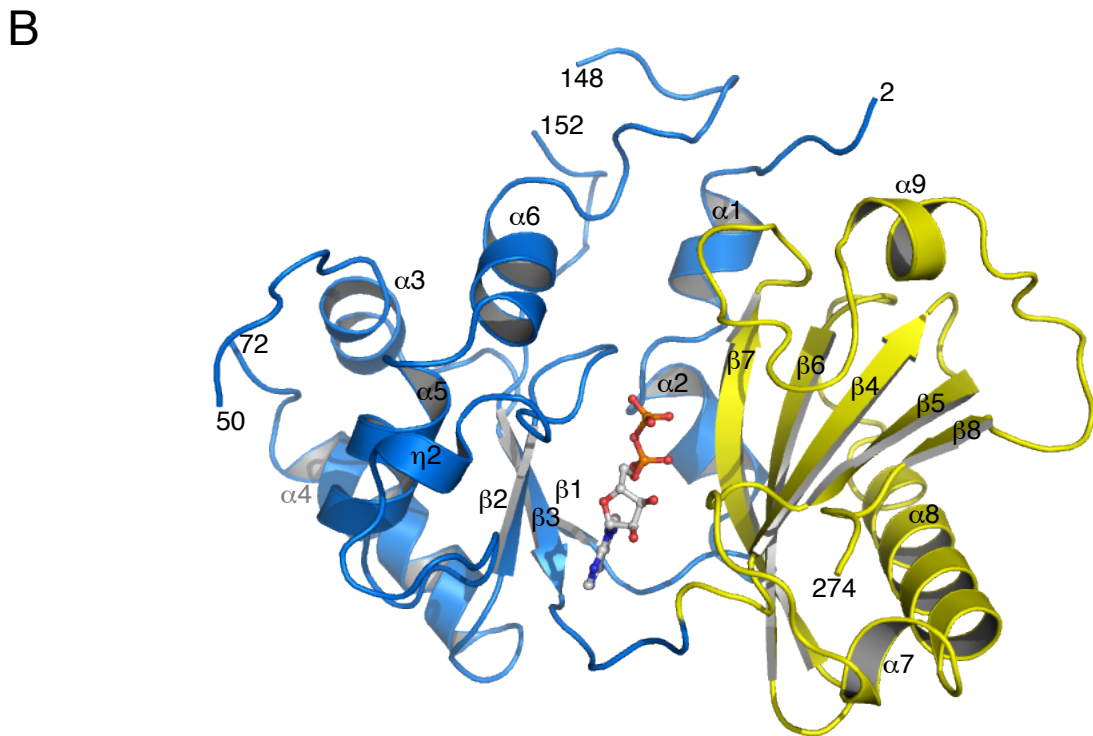
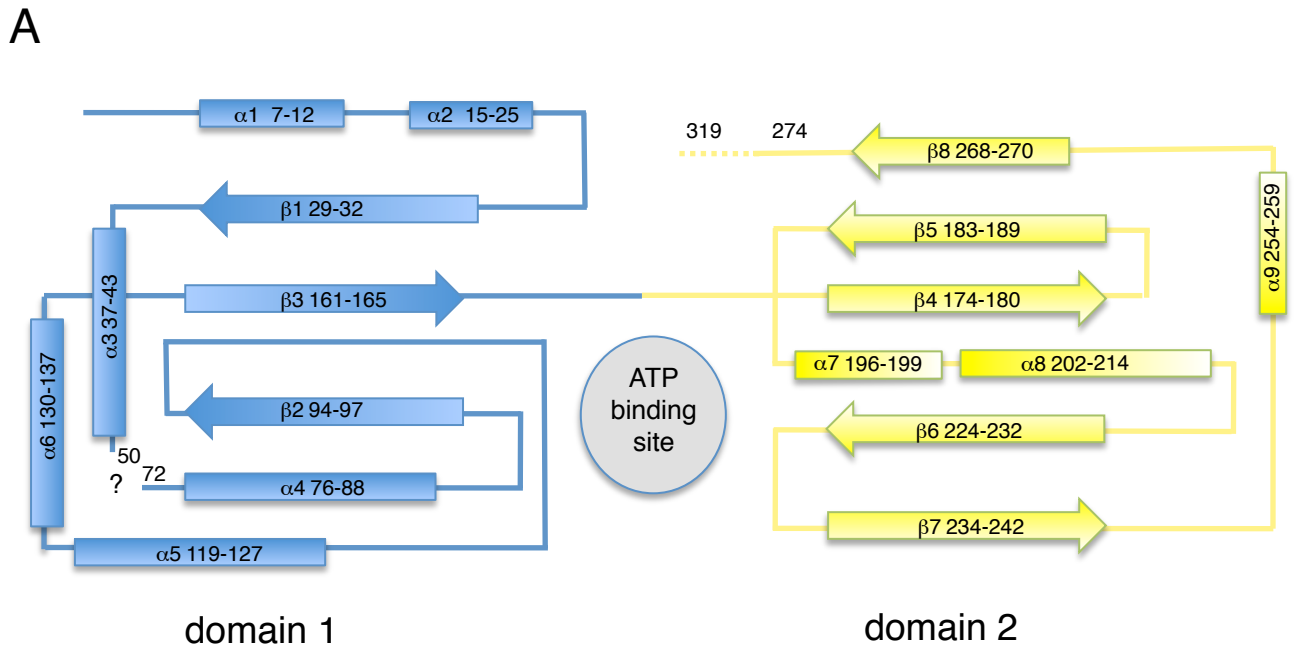


Figure 2

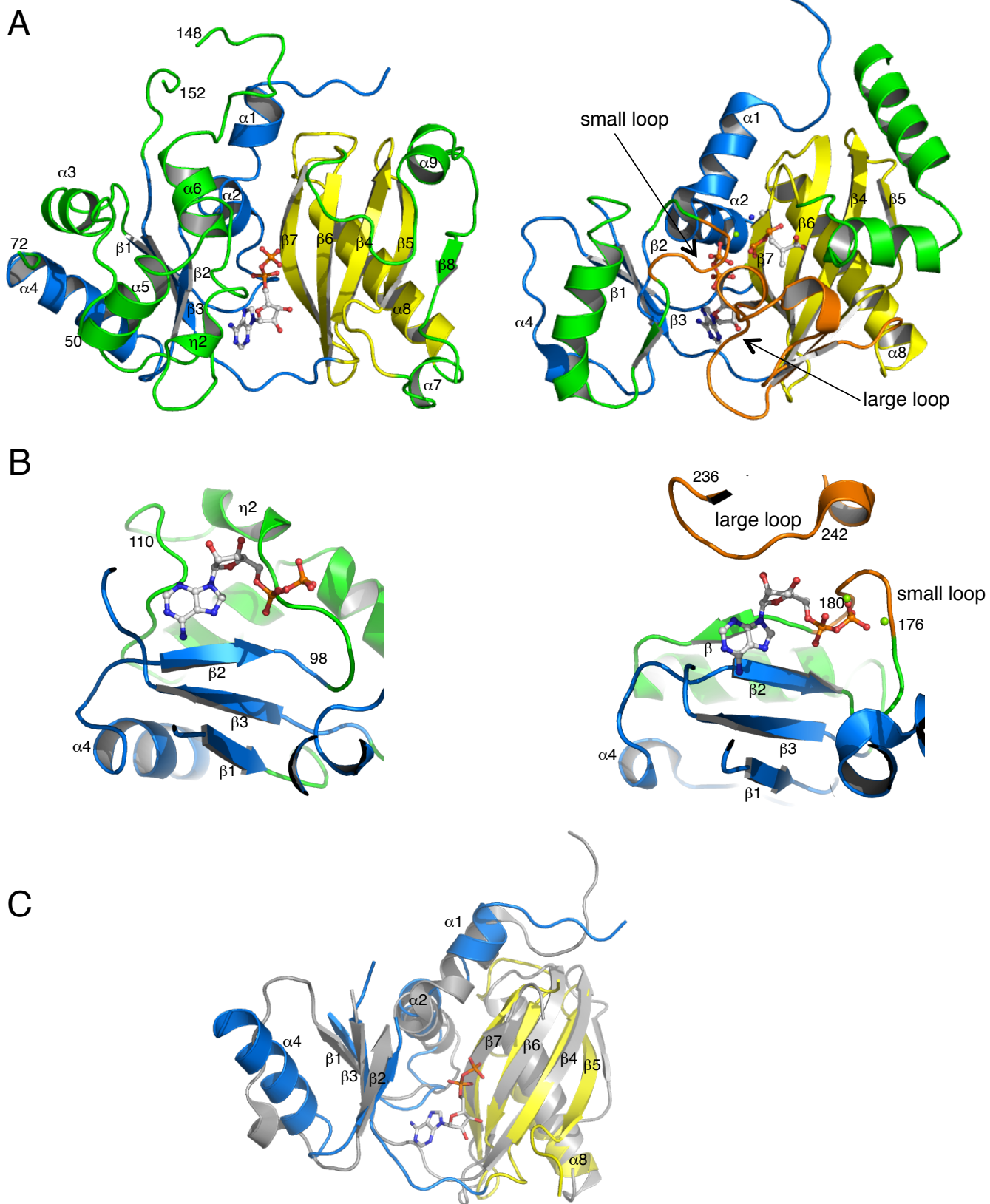
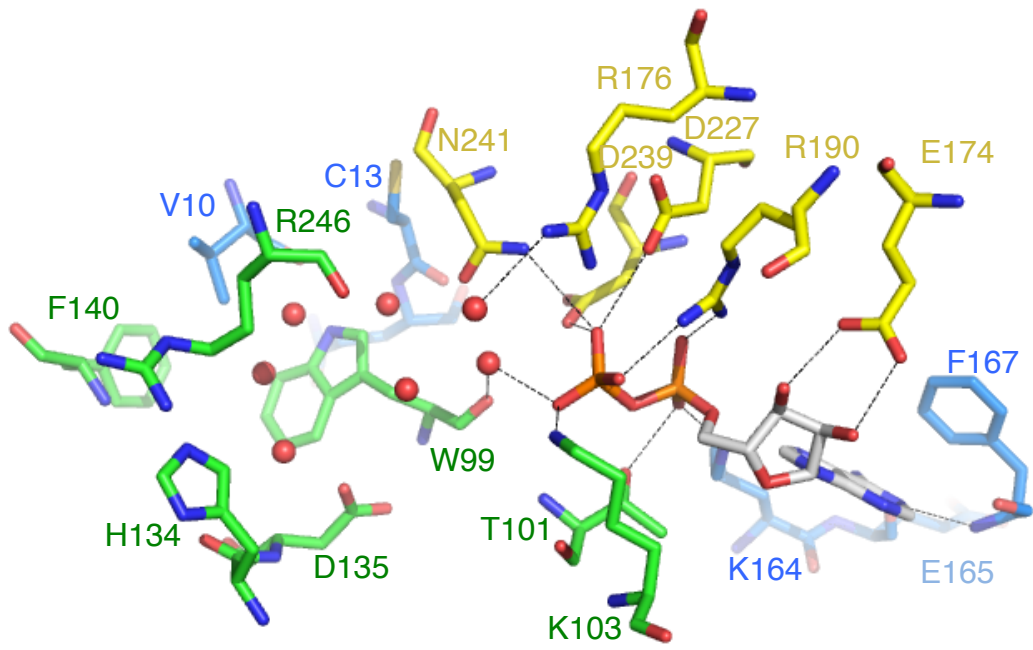


Figure 3

A



B

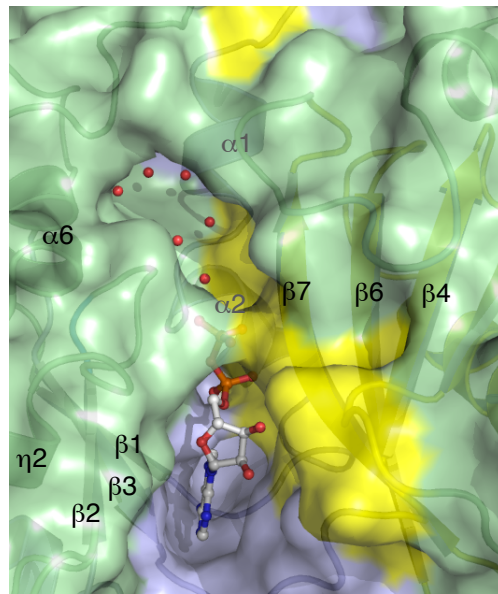


Figure 4

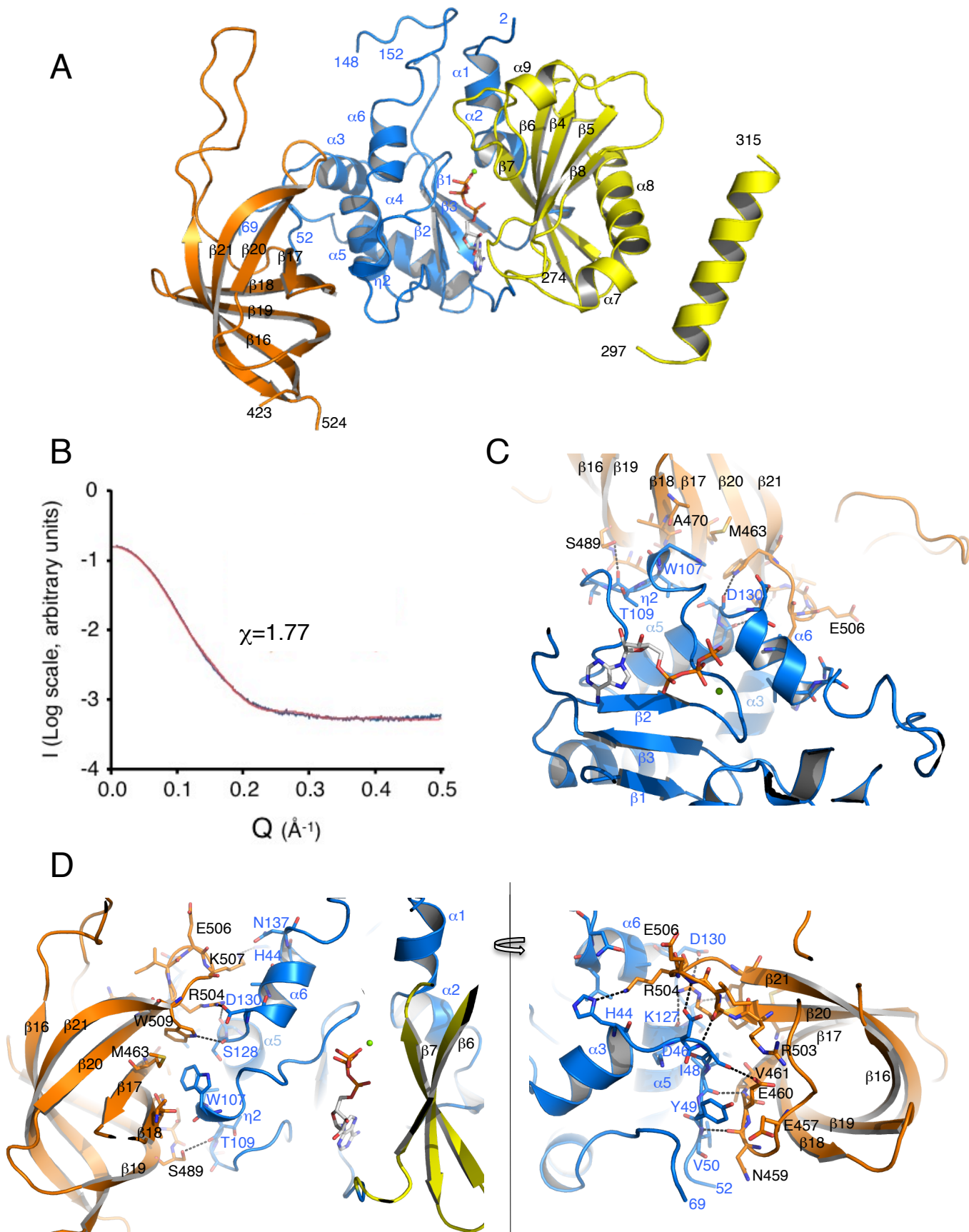
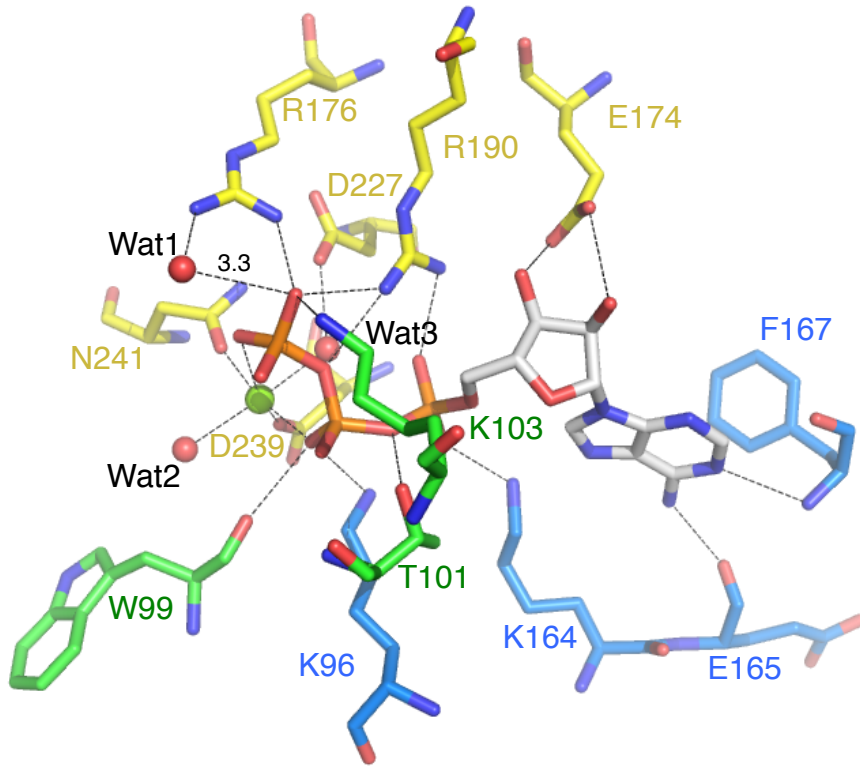


Figure 5

A



B

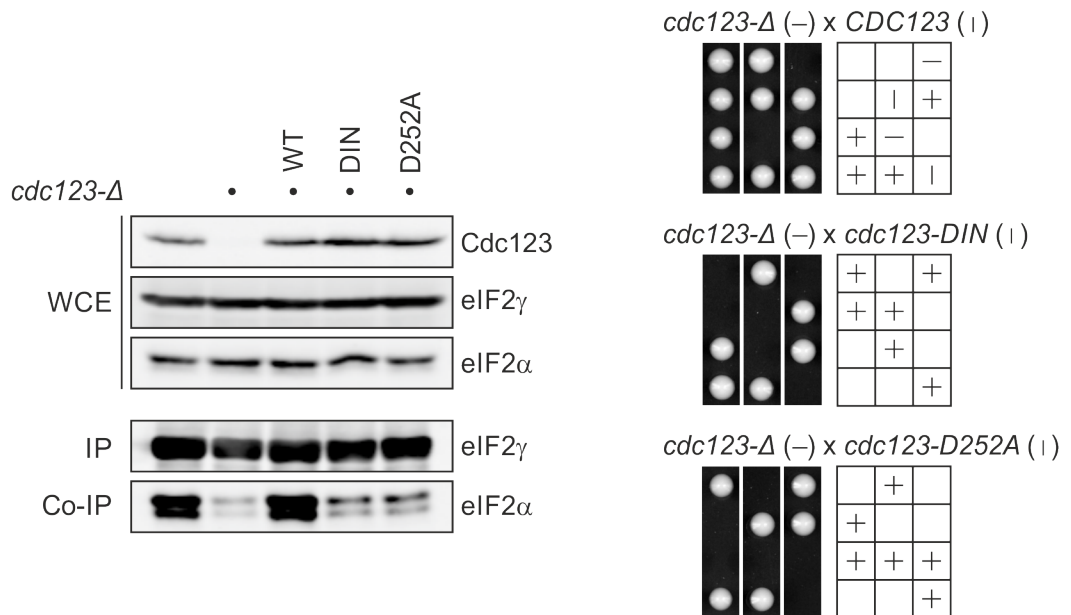
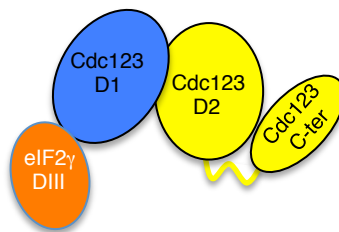
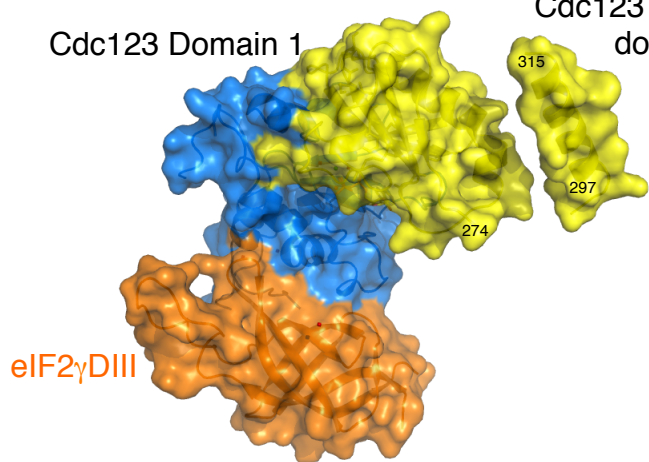


Figure 6

A

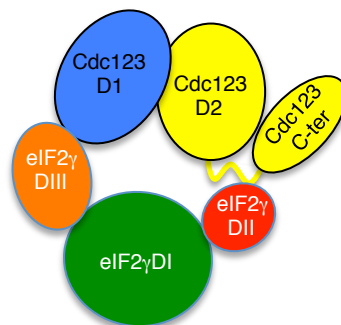
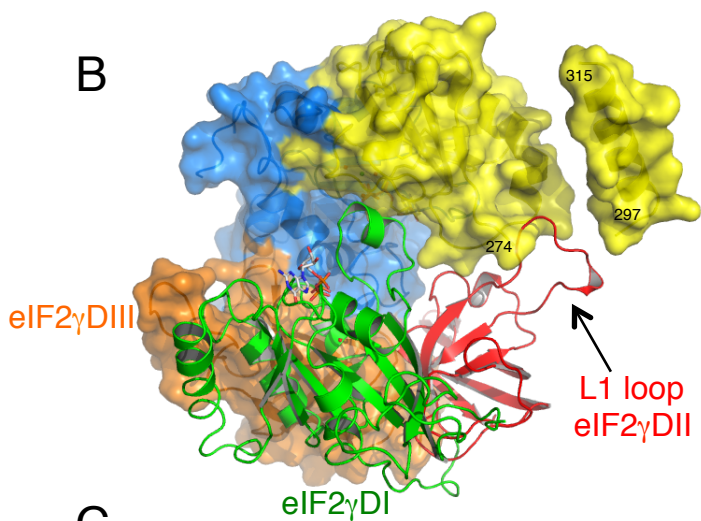
Cdc123 Domain2 Cdc123 C-terminal domain

Cdc123 Domain 1



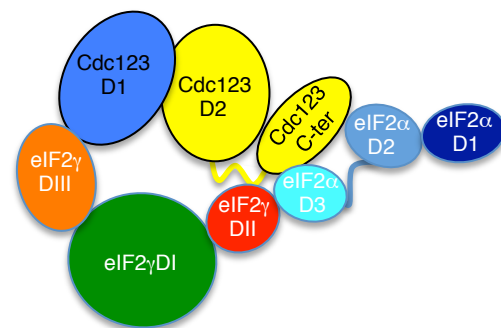
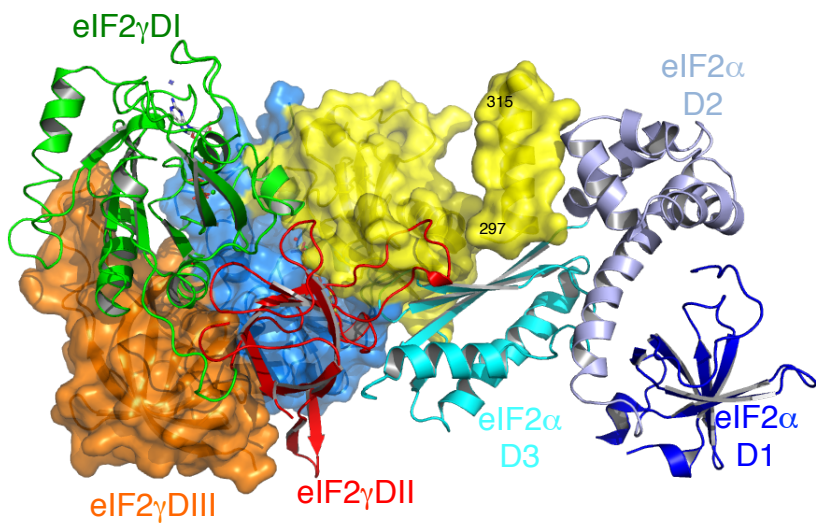
Cdc123-eIF2γDIII complex:  
« pre-assembly complex »

B



Cdc123-eIF2γ complex

C



Catalytic complex-eIF2α<sub>γ</sub>  
assembly

<b>Data Collection</b>	Sp-Cdc123Δc	Sp-Cdc123Δc +ADP	Sp-Cdc123:Sc-γDIII +ATP-Mg <sup>2+</sup>	Sp-Cdc123:Sc-γDIII
Crystallization Conditions	4% tacsimate pH 5.0 12%PEG3350	4% tacsimate pH5.0 12%PEG3350	0.2M LiSO4 0.1M Tris pH 8.0 25%PEG3350	0.2M LiSO4 0.1M Tris pH 8.0 25%PEG3350
Space group	C2	C2	C222 <sub>1</sub>	C222 <sub>1</sub>
Cell dimensions				
<i>a, b, c</i> (Å)	85.6 91.7 86.2	86.5 91.4 86.0	74.3 116.6 132.6	75.0 117.4 132.4
<i>α, β, γ</i> (°)	90 93.5 90	90 91.4 90	90 90 90	90 90 90
Resolution (Å)	45.8-2.06	43.2-1.85	45.0-2.9	45.7-3.0
<i>R</i> <sub>sym</sub> (%)	5.0 (90.8) <sup>a</sup>	3.3 (47.4)	7.4 (87.5)	10.2 (117.3)
<i>I</i> / <i>σI</i>	15.7 (1.3)	19.0 (2.7)	15.8 (2.2)	13.4 (2.0)
CC1/2 (%)	99.9 (77.5)	99.9 (78.6)	99.9 (80.4)	99.9 (87.4)
Completeness (%)	99.0 (94.3)	98.1 (96.4)	99.7 (99.3)	99.6 (97.8)
Redundancy	5.5 (5.1)	3.0 (2.9)	5.8 (5.9)	7.3 (7.0)
<b>Refinement</b>				
Resolution (Å)	45.8-2.06	43.2-1.85	45.0-2.9	45.7-3.0
No. reflections	41180	56270	13237	12020
<i>R</i> <sub>work</sub> / <i>R</i> <sub>free</sub>	0.193 (0.230)	0.183 (0.221)	0.195 (0.262)	0.218 (0.257)
No. atoms/B-factors (Å <sup>2</sup> )				
Protein	Mono1Cdc123 2075/57.9	Mono1Cdc123 2096/35.5	Cdc123 2288/101.7	Cdc123 2234/110.3
	Mono2Cdc123 2060/66.4	Mono2Cdc123 2048/44.0	γD3 805/100.0	γD3 798/100.3
Water	198/62.5	331/44.3	5/72.8	
Ligand		ADP-mono1/27/38.4	ATP 31/82.1 Mg 1/72.6	
R.m.s. deviations				
Bond lengths (Å)	0.008	0.008	0.009	0.008
Bond angles (°)	1.09	1.10	1.18	1.05

**Table 1:** Data collection and refinement statistics for Sp-Cdc123 structure determination

A single crystal was used for data collection.

<sup>a</sup>Values in parentheses are for highest-resolution shell.

Sp-Cdc123	Sc- $\gamma$ DIII	distances (Å)
Electrostatic bonds		
H44 N $\delta$ 1	K507 N $\zeta$	3.1
D46 O $\delta$ 2	E506 N (mc)	3.0
S47 O $\gamma$	E460 O $\epsilon$ 2	3.2
I48 O (mc)	V461 N (mc)	2.7
V50 N (mc)	N459 O (mc)	3.0
S47 N (mc)	R504 O (mc)	2.8
K127 O	R504 Nh1	3.3
D130 O $\delta$ 1	R504 Nh2	2.7
S128 O (mc)	W509 N $\epsilon$	3.3
Non-bonded contacts		
Y49	E457	
W107	M463-A470-T471- G472	
I108	T488-S489	
T109	T488-S489	
T110	T488-S489	
A133	K507	
L136	K507	
N137	K507	
L43	K507	
S47	R503	
D46	I505	

**Table 2:** Summary of interactions involved in the binding of  $\gamma$ DIII domain to Cdc123. Residue names are colored according to Figure S2.

Sp-Cdc 123	ATP binding Sp-Cdc123:Sc- $\gamma$ DIII	distances (Å)
Electrostatic bonds		
K96 N $\zeta$	O1 $\alpha$	2.9
	O2 $\beta$	3.3
T101 O $\gamma$ 1	O3 $\alpha$	3.0
	O1 $\beta$	2.8
K164 N $\zeta$	O1 $\alpha$	2.8
	N7 adenine	2.9
E165 O (mc)	N6 adenine	3.0
F167 N (mc)	N1 adenine	3.2
E174 O $\epsilon$ 1	O2' ribose	3.3
O $\epsilon$ 2	O3' ribose	2.9
R176	O3 $\gamma$	3.0
R190 Nh1	O2 $\alpha$	2.8
Nh2	O3 $\gamma$	2.9
D227 O $\delta$ 2	Wat3	2.7
D239 O $\delta$ 2	Mg <sup>2+</sup>	2.1
	O2 $\beta$	2.9
N241 O $\delta$ 1	Mg <sup>2+</sup>	2.2
Wat2	Mg <sup>2+</sup>	2.7
Wat3	Mg <sup>2+</sup>	2.5
Non-bonded contacts		
K103	O1 $\gamma$	
	O1 $\beta$	
S100	O1 $\gamma$	
	O1 $\beta$	
I238	O1 $\beta$	
	O2 $\beta$	
L114	O4' ribose	
W166	N6 adenine	
	N1 adenine	
	C2 adenine	
V94	N6 adenine	
M169	C8 adenine	
	N7 adenine	
	C5 adenine	

**Table 3:** Summary of interactions involved in the binding of ATP to Sp-Cdc123:Sc- $\gamma$ DIII.

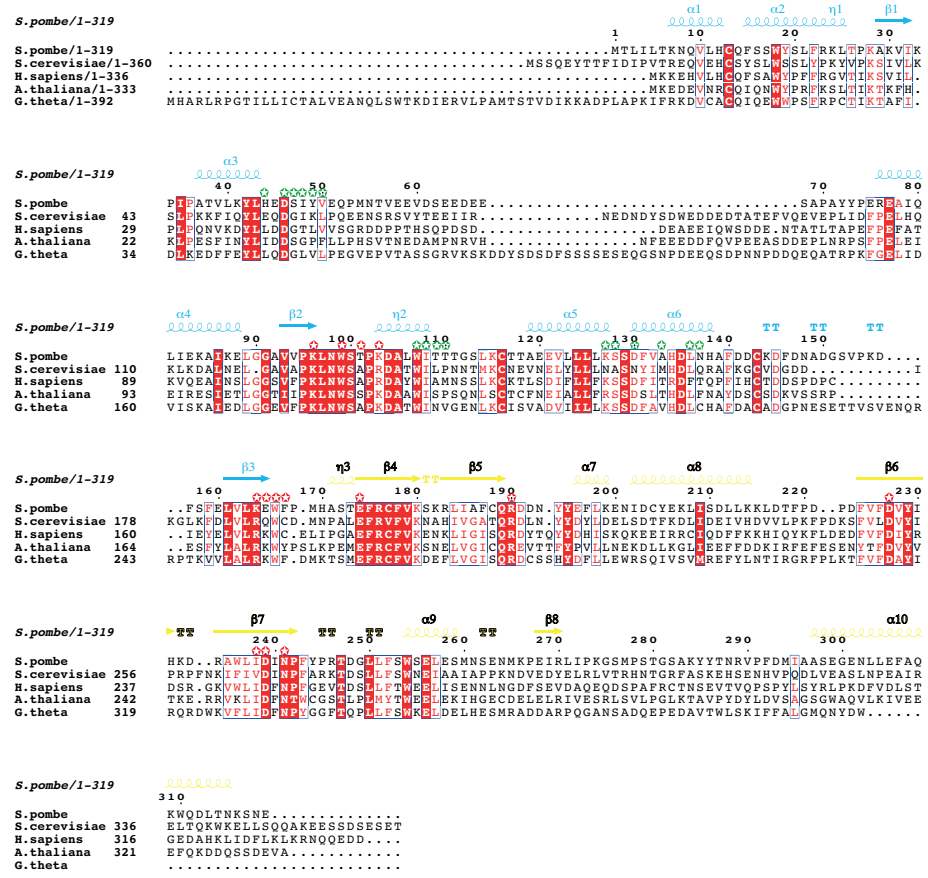
Residue names are colored according to Figure S2.

**Supplemental Data**

1  
2  
3  
4  
5  
6  
7  
8  
9  
10  
11  
12  
13  
14  
15  
16  
17  
18  
19  
20  
21  
22  
23  
24  
25  
26  
27  
28  
29  
30  
31  
32  
33  
34  
35  
36  
37  
38  
39  
40  
41  
42  
43  
44  
45  
46  
47  
48  
49  
50  
51  
52  
53  
54  
55  
56  
57  
58  
59  
60  
61  
62  
63  
64  
65

**Supplemental Figures and Legends**

A



B

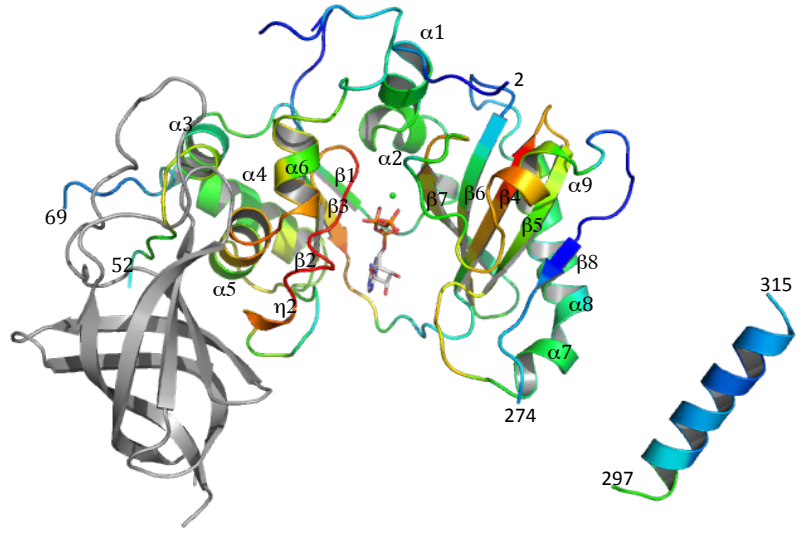


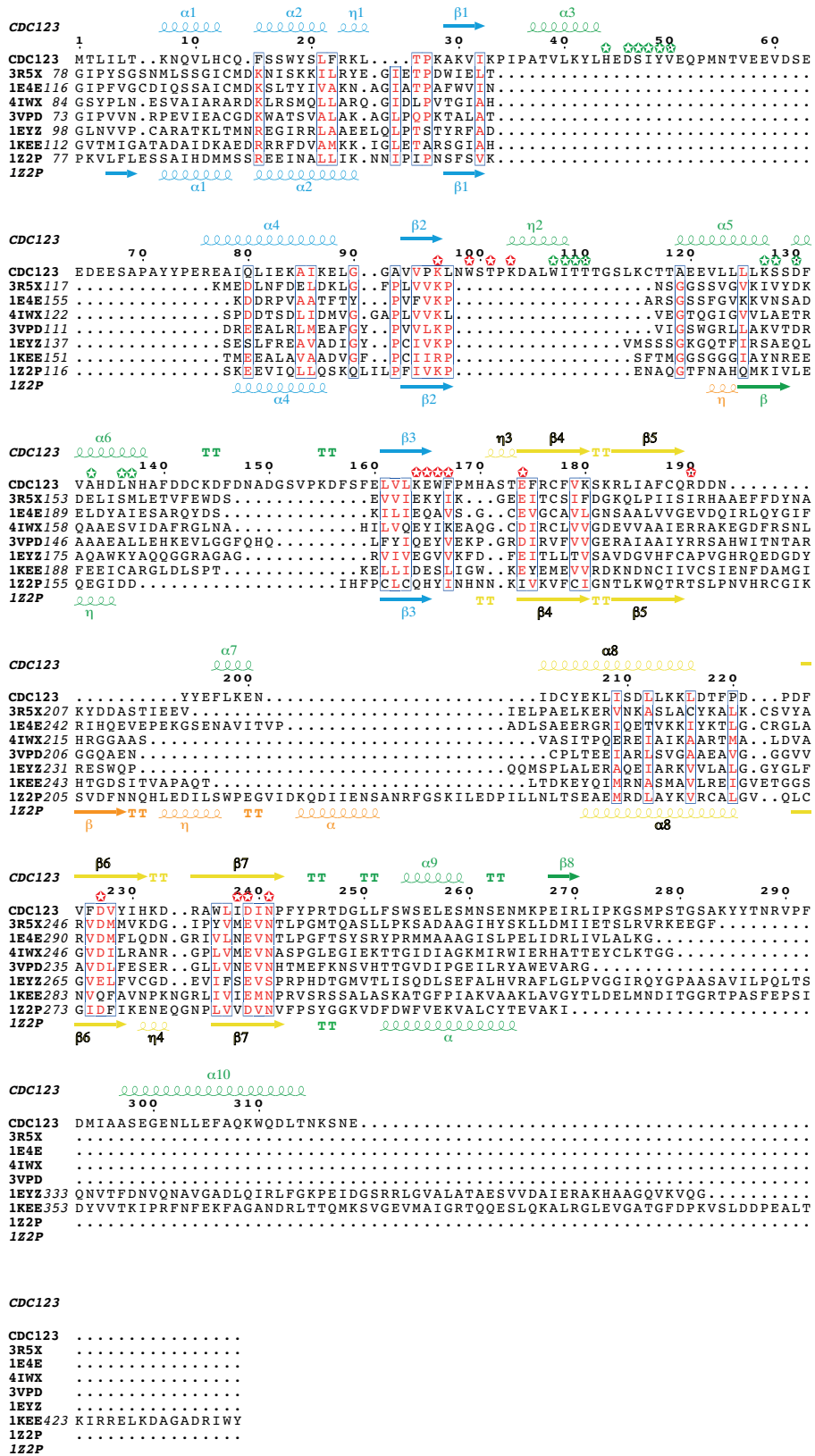
Figure S1: Sequence conservation among Cdc123 orthologs

A-c.a 200 sequences of Cdc123 orthologs were aligned using ClustalW (Larkin et al., 2007). The consensus sequence was calculated using JalView (Waterhouse et al., 2009). The figure was drawn

1 with Espript (Gouet et al., 1999) and edited manually. For the sake of clarity, only five representative  
2 Cdc123 sequences are shown. Residues conserved in 78-100% of the sequences are in white letters in  
3 red boxes. Residues conserved in 50-77% of the sequences are in red letters and boxed. Residues  
4 involved in ATP binding to Sp-Cdc123 are indicated with stars boxed in red. Residues involved in the  
5 binding of Sc- $\gamma$ DIII domain to Sp-Cdc123 are indicated with stars boxed in green. Secondary  
6 structures of Sp-Cdc123 are shown at the top of the alignment.  
7  
8  
9  
10  
11  
12

13 B-From the above alignment, conservations at each position were analyzed by using Jalview. The  
14 PAM 250 similarity matrix was used in this step. Residues on Cdc123 were colored according to the  
15 similarity score with a linear scale from blue to red (rainbow scale of PyMol). The  $\gamma$ DIII domain was  
16 colored in grey.  
17  
18  
19  
20  
21  
22  
23  
24  
25  
26  
27  
28  
29  
30  
31  
32  
33  
34  
35  
36  
37  
38  
39  
40  
41  
42  
43  
44  
45  
46  
47  
48  
49  
50  
51  
52  
53  
54  
55  
56  
57  
58  
59  
60  
61  
62  
63  
64  
65

# A



B

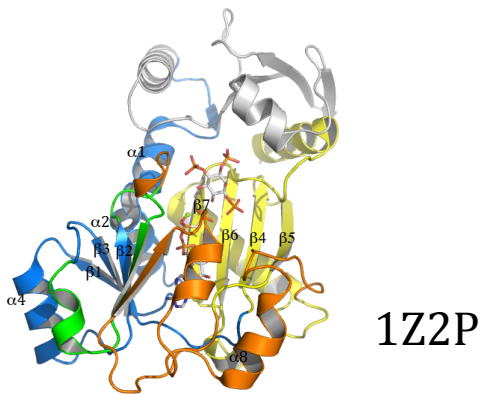
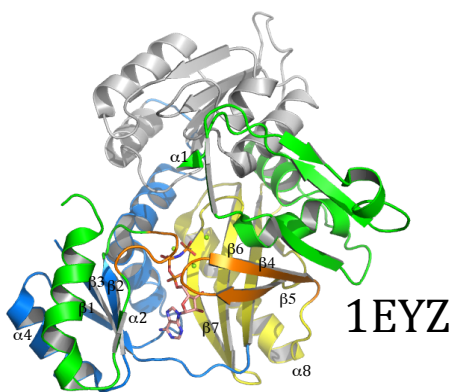
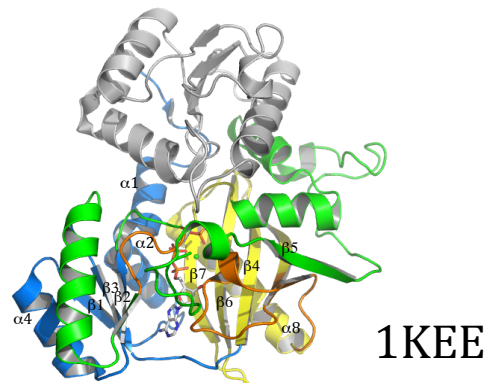
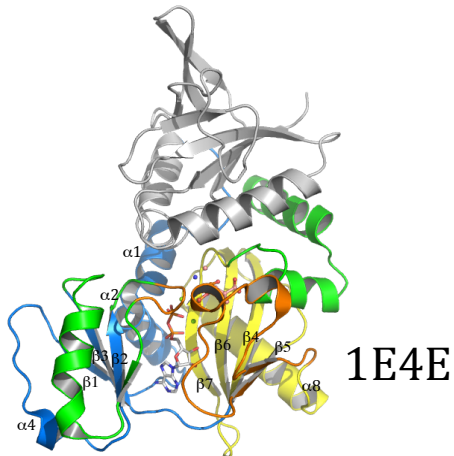
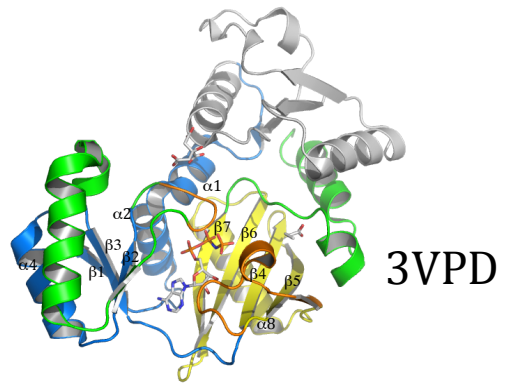
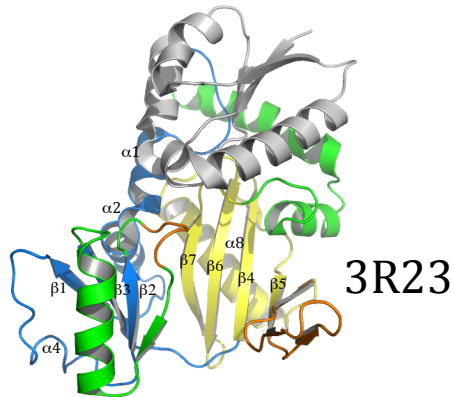
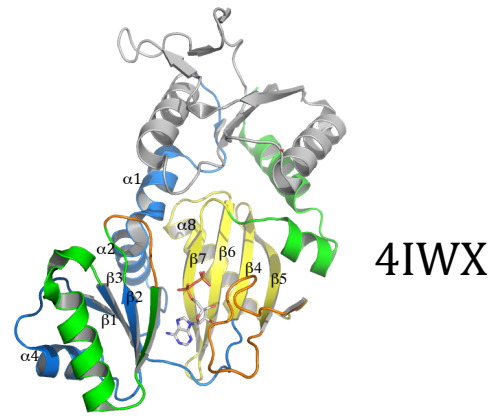
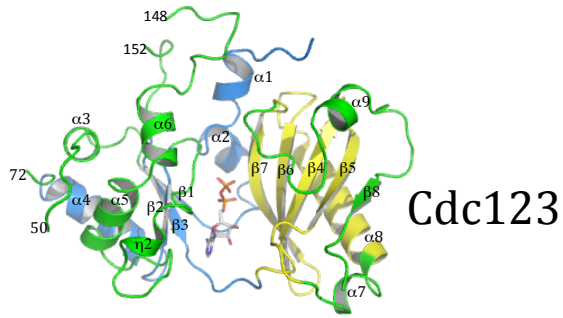
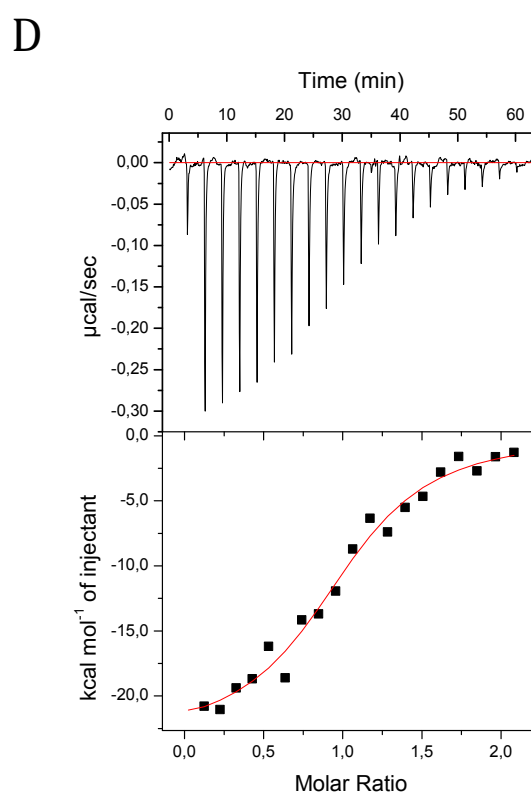
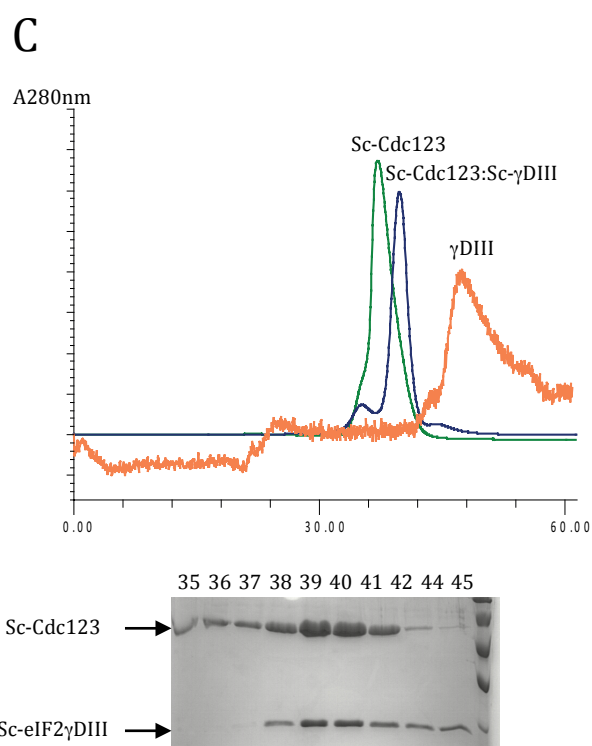
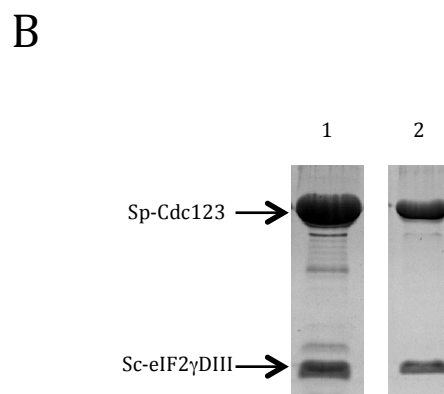
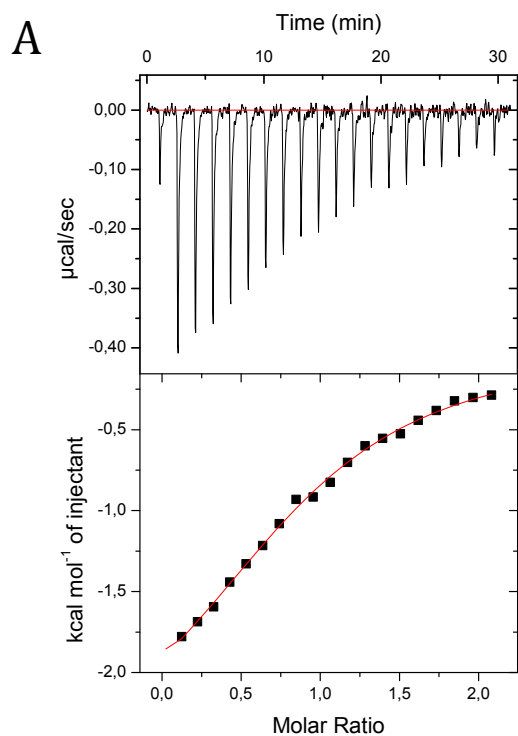


Figure S2: Structural alignment of sp-Cdc123 with enzymes from ATP-grasp superfamily

1 A- The sequence of Sp-Cdc123 was aligned to those of some ATP-Grasp enzymes according to the  
2 structural superimpositions. Secondary structure of Sp-Cdc123 is indicated at the top of the alignment.  
3  
4 Secondary structure of Inositol 1,3,4-trisphosphate 5/6-Kinase (PDB ID code 1Z2P; (Miller et al.,  
5 2005)) is indicated at the bottom of the alignment. Color code for the secondary structure elements is  
6 the same as in Figures 2 and S4. Conserved residues are boxed and colored in red. Residues involved  
7 in ATP binding to Sp-Cdc123 are indicated with stars boxed in red. Residues involved in the binding  
8 of Sc- $\gamma$ DIII domain to Sp-Cdc123 are indicated with stars boxed in green. The figure was drawn with  
9 Esprout (Gouet et al., 1999). Sequences are labeled according to the ID code of the corresponding PDB  
10 entry.  
11  
12  
13  
14  
15  
16  
17  
18  
19

20 B- Structural comparison of sp-Cdc123 with enzymes belonging to the ATP-grasp superfamily.  
21 Color code is as follows: in Cdc123, domain 1 is colored in blue and domain 2 is colored in yellow. In  
22 ATP-Grasp enzymes, domain N is colored in grey, the central domain is colored in blue and the C-  
23 terminal domain is colored in yellow. Divergent regions in Cdc123 and ATP-grasp are shown in  
24 green. Ligands are shown with sticks when available. The small and large loops overhanging ATP in  
25 ATP-Grasp are shown in orange. Regions specific to Cdc123 proteins are colored in green. ATP is  
26 shown in sticks. Secondary structures common to Cdc123 and ATP-grasp are labeled. The PDB code  
27 of each represented ATP-grasp structure is indicated on the right of the cartoon. 4IWX, RimK, (Zhao  
28 et al., 2013)  $rms_d$  of 3.6 Å over 156 C $\alpha$  atoms ( $Z=8.3$ ); 3R23, D-alanine-D-alanine ligase,  $rms_d$  of 3.2  
29 Å over 160 C $\alpha$  atoms ( $Z=11.2$ ); 3VPD, LysX, (Ouchi et al., 2013)  $rms_d$  of 3.7 Å over 160 C $\alpha$  atoms  
30 ( $Z=9.6$ ); 1E4E, D-alanyl-D-lactate ligase (Roper et al., 2000)  $rms_d$  of 3.6 Å over 169 C $\alpha$   
31 atoms ( $Z=9.7$ ); 1KEE, carbamoyl phosphate synthetase (Miles et al., 2002)  $rms_d$  of 3.3 Å over 179 C $\alpha$   
32 atoms ( $Z=9.1$ ); 1EYZ, Glycimanide ribonucleotide transformylase (Thoden et al., 2000)  $rms_d$  of 3.3 Å  
33 over 175 C $\alpha$  atoms ( $Z=9.1$ ); 1Z2P, Inositol 1,3,4-trisphosphate 5/6-Kinase (Miller et al., 2005)  $rms_d$   
34 3.1 Å over 166 C $\alpha$  atoms ( $Z=10.0$ ).  
35  
36  
37  
38  
39  
40  
41  
42  
43  
44  
45  
46  
47  
48  
49  
50  
51  
52  
53  
54  
55  
56  
57  
58  
59  
60  
61  
62  
63  
64  
65



**Figure S3: Biochemical characterization of Cdc123**

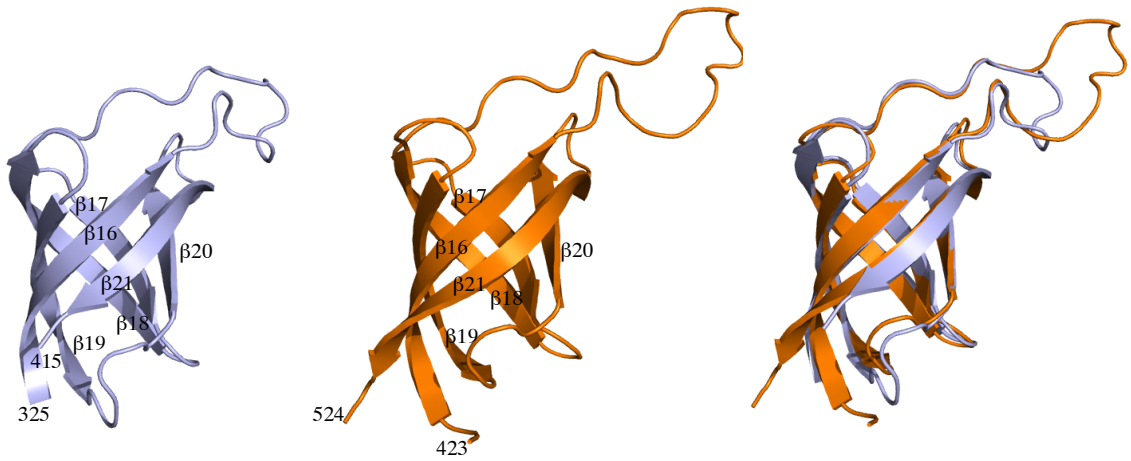
A-Titration curve (upper panel) and binding isotherm (lower panel) of Sp-Cdc123 interaction with ATP-Mg<sup>2+</sup> at 25°C. The K<sub>d</sub> value derived from the curve is 67 ± 13 µM.

1 B-SDS-PAGE analysis of the purification of the Sp-Cdc123:Sc- $\gamma$ DIII complex. Lane 1: sample  
2 obtained after the affinity chromatography step. Lane 2: sample obtained after molecular sieving.  
3

4 C-Upper part: Overlay of elution profiles on molecular sieve (Superdex 200 HR 10/30) of Sc-Cdc123  
5 (green), Sc-Cdc123:Sc- $\gamma$ DIII complex (blue) and Sc- $\gamma$ DIII (orange). Lower part: SDS-PAGE analysis  
6 of elution profile of Sc-Cdc123:Sc- $\gamma$ DIII complex (blue curve in upper panel). The number of each  
7 fraction is indicated (one fraction was collected every minute, 0.4 mL/min flow rate).  
8  
9  
10  
11  
12

13 D-Titration curve (upper panel) and binding isotherm (lower panel) of Sc-Cdc123 interaction with Sc-  
14  $\gamma$ DIII at 25°C. The K<sub>d</sub> value derived from the curve is  $2.5 \pm 0.5 \mu\text{M}$ .  
15  
16  
17  
18  
19  
20  
21  
22  
23  
24  
25  
26  
27  
28  
29  
30  
31  
32  
33  
34  
35  
36  
37  
38  
39  
40  
41  
42  
43  
44  
45  
46  
47  
48  
49  
50  
51  
52  
53  
54  
55  
56  
57  
58  
59  
60  
61  
62  
63  
64  
65

A



B

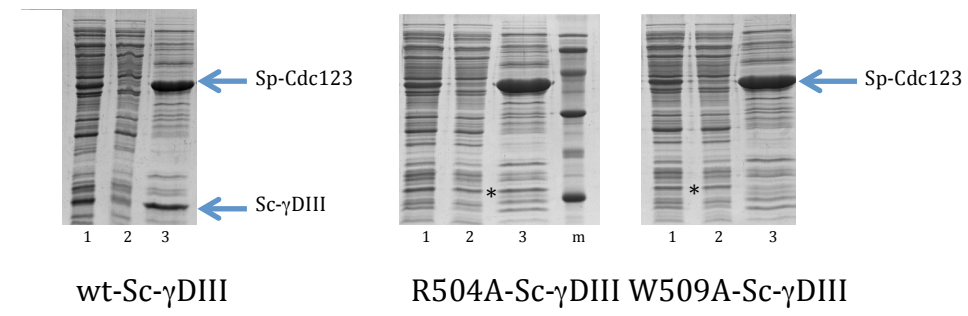
*S. cerevisia/423-527*

	β16	T · T	TT	β17	β18
<i>S. cerevisia/423-527</i>	432	442	452	462	472
<i>S. cerevisia/423-527</i>	LPNITYTDEINNYFLLRRLRGVKT.DGQKQAKVRLLEPNVLMVNIIGSTAGARVVAVKAD				
<i>S. pombe/344-446</i>	LPEVYTELEINNYFLLRRLRGVKS.GDKNTTKVQKLAKNVLVNIIGSTAGGRVMMVKAD				
<i>A. thaliana/356-465</i>	LPDVFVLELVNFLLRRLRGVRTKGSQKQKVKSLTKGELMLNIIGSTMAGAKVGVVKVD				
<i>C. aretis/367-475</i>	LPSIFIELEVSYYLLKRLRGVMEGDKKQAKVQRLSKSEVLLVNIIGSTAGGRVATKAD				
<i>L. decemlineata/365-471</i>	LPSIFIELEVSYYLLKRLRGVMEGDKKQAKVQRLSKSEVLLVNIIGSTAGGRVATKAD				
<i>M. musculus/363-471</i>	LPEITFTELEISYFLLRRLRGVTEGDKKAKAKVQRLSKNVLVNIIGSTAGGRVSAVKAD				
<i>D. melanogaster/363-475</i>	LPDIYQELLEISYFLLRRLRGVRTDGGDKKQAKVQRLQKNVLLVNIIGSTAGGRISATKGD				
<i>C. elegans/363-469</i>	LPDIFIELEISFYLLRRLRGVTEGDKKQAKVQRLVKEVLLVNIIGSTAGGRVAVKGD				
<i>G. theta/389-491</i>	LPPIVSKILINRYRLLKRLFLSK.D.S.IKSVGIKLGEIIMITVNNSSGKIYSKKKN				
<i>E. cuniculi/331-439</i>	LPSIFHKITVEYSLFPKTTIQGS.SNLK.EGHHVLLNIIGSTAGSVIGRINET				
<i>M. jannaschii/345-437</i>	LPPIREKITIRANLLDRVVGTKE.E.LKIEPLRTGVLMLNIGTATAGVITSAAGD				
<i>M. thermoauto./317-408</i>	LPPVRSFTMETHLLERVVGTKE.E.TKVEPIKTGEPMLNIVGTTAGVIVKSARAD				
<i>A. fulgidus/333-424</i>	LPDVLSFTMEVNLLERVVGLDE.E.MEVKIKMNEPMLAVGTATILGIVTSARAD				
<i>H. halobium/321-414</i>	LPPTWESFEMVDLLERLVGA.AA.EAEQIDDISTGEPMLPVGTATIVGIVTSARAD				
<i>T. volcanium/317-411</i>	VPPISFMRLEAHLKRVVGSQD.E.LNVVPIRAKTLMTVATANVGVVSNVKGIT				
<i>T. acidophilum/317-411</i>	VPPVAFSMRLESHLKRVVGSQD.E.LNVVPIRPKTLMTVATANVGVVSNVKGIT				
<i>P. abyssi/319-411</i>	LPPVWDSLRLREVHLERVVGTQ.E.LKVEPIKRRVLLNIGTARMLGLVTGLGKD				
<i>A. pernix/324-420</i>	LPEPLTLRIEHHLEKVVGMKE.E.ARVVPIRRGEMLLSVGTATILGIVTSARAD				
<i>S. solfataricus/322-415</i>	EVPLWNLIRIKYNLLERVVGAKE.E.MLKVDPIRAKTLMLSVGSSITLGLIVTSVKKD				

*S. cerevisia/423-527*

	β19	T · T	β20	β21
<i>S. cerevisia/423-527</i>	492	502	512	522
<i>S. pombe/344-446</i>	MARLQTSFACFEI.NEKIALSRRIEKHWRLIGWATIKKGTTLPEIA.EK			
<i>A. thaliana/356-465</i>	LAKLQTSFACFEI.GEKVALSRRIEKHWRLIGWAKVVEGKTLKV.EK			
<i>C. aretis/367-475</i>	LCKIATSNPVCTEI.GEKIALSRRIEKHWRLIGWQIRGGETIEPSSNLT.EK			
<i>L. decemlineata/365-471</i>	LCKIATSNPVCTEI.GEKIALSRRIEKHWRLIGWQIRGGETIEPSSNLT.EK			
<i>M. musculus/363-471</i>	LGKIATSNPVCTEI.GEKIALSRRIEKHWRLIGWQIRRGVTIKPTVDDD.EK			
<i>D. melanogaster/363-475</i>	LAKIVLTSNPVCTEK.GEKIALSRRIENHWRLIGWQIRFGKTIPTVLDVQVAKK.EK			
<i>C. elegans/363-469</i>	AAKIRLNDPICTEF.GEKIAMSRRIEKHWRLIGWQIRKQGTVEPYKN.EK			
<i>G. theta/389-491</i>	NVSIETIKPICNF.SDKVCISRRINNHWRVLCGCTISKLNNMNVFN.EK			
<i>E. cuniculi/331-439</i>	SGEFDVVKPACFEI.GERIAISRRIENHWRLIGHGEIKDGTCEIPEYDAEIDDAQRKAD			
<i>M. jannaschii/345-437</i>	IADIKLKLPICAEIGDRVAISRRIENHWRLIGVGTIEG.EK			
<i>M. thermoauto./317-408</i>	DADVVKLPAEAE.GORIALSRVGAHWRLIGVGIK.EK			
<i>A. fulgidus/333-424</i>	IVEVKLRRPVCADK.GSRVAISRRIENHWRLIGVGIK.EK			
<i>H. halobium/321-414</i>	ECEVALKRRPVCAPA.GKIAISRRIENHWRLIGVGTIESE.EK			
<i>T. volcanium/317-411</i>	DIEVSLKYPVAAFN.GMRVAISRRIENHWRLIGVGIQSLE.EK			
<i>T. acidophilum/317-411</i>	EIEVSLKYPVAAFN.GMRVAISRRIENHWRLIGVGIQSLE.EK			
<i>P. abyssi/319-411</i>	EIEVSLQIPVCAEP.GDRVAISRRIENHWRLIGVGIKE.EK			
<i>A. pernix/324-420</i>	EIEVQLRRPVVWTP.KARVALSRRIENHWRLIGWGLIK.EK			
<i>S. solfataricus/322-415</i>	EIEVQLRRPVVWSNN.RTVISRRIENHWRLIGWGLVEI.EK			

C



wt-Sc-γDIII R504A-Sc-γDIII W509A-Sc-γDIII

**Figure S4: e/aIF2 $\gamma$ DIII domain.**

A-Cartoon representation of the  $\gamma$ DIII domain. Left part: aIF2 $\gamma$ DIII domain from *S. solfataricus* (PDB ID Code 2AHO, (Yatime et al., 2006)) colored in light blue. Middle part: eIF2 $\gamma$ DIII domain from *S. cerevisiae* as determined in this study, colored in orange. Right part: Superimposition of both structures ( $rms_d=0.69\text{\AA}$  over 79 C $\alpha$  atoms). Secondary structures are labeled according to (Yatime et al., 2006).

B-Alignment of e/aIF2- $\gamma$ DIII domains sequences. 10 sequences of eukaryotic eIF2 $\gamma$  and 9 sequences of archaeal aIF2 $\gamma$  (framed in blue) were aligned using ClustalW (Larkin et al., 2007). The figure was drawn with Esript (Gouet et al., 1999). When the percentage of identity is higher than 70%, residues are colored in red and framed in blue. In case of strict identity, residues are in white on a red background. Residues involved in the binding of Sc- $\gamma$ DIII domain to Sp-Cdc123 are indicated with stars boxed in green. Secondary structures of Sc- $\gamma$ DIII are indicated at the top of the alignment and those of Ss-aIF2- $\gamma$ DIII are indicated at the bottom.

C- Binding assay of Sc- $\gamma$ DIII to Sp-Cdc123.

The pull-down binding assay is described in the Material and Methods section. An equal aliquot of each step of the batch purification (Talon affinity resin) was loaded onto a 12% polyacrylamide SDS gel. Stars indicate the position of Sc- $\gamma$ DIII.

Lane 1: soluble fraction of the crude extract

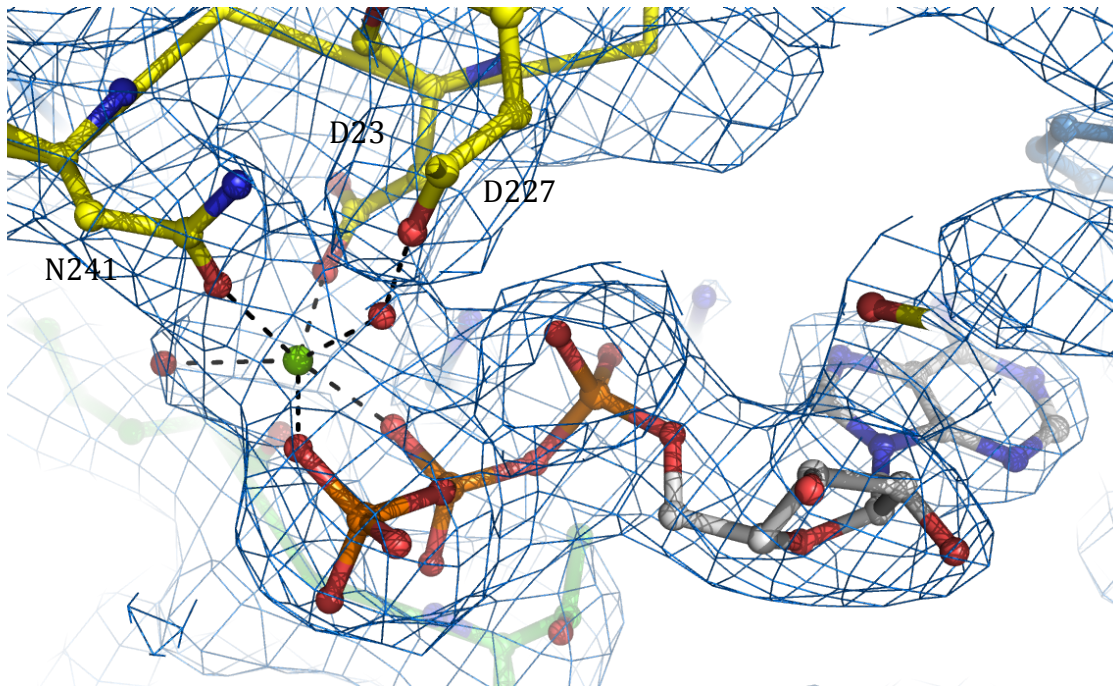
Lane 2: flow-through fraction of the batch purification

Lane 3: elution fraction of the batch purification

M:molecular weight marker (97, 67, 43, 30, 20, 14 kDa; GE Healthcare)

The views show that R504 and W509 mutants have lost some ability to bind Sp-Cdc123.

A



B

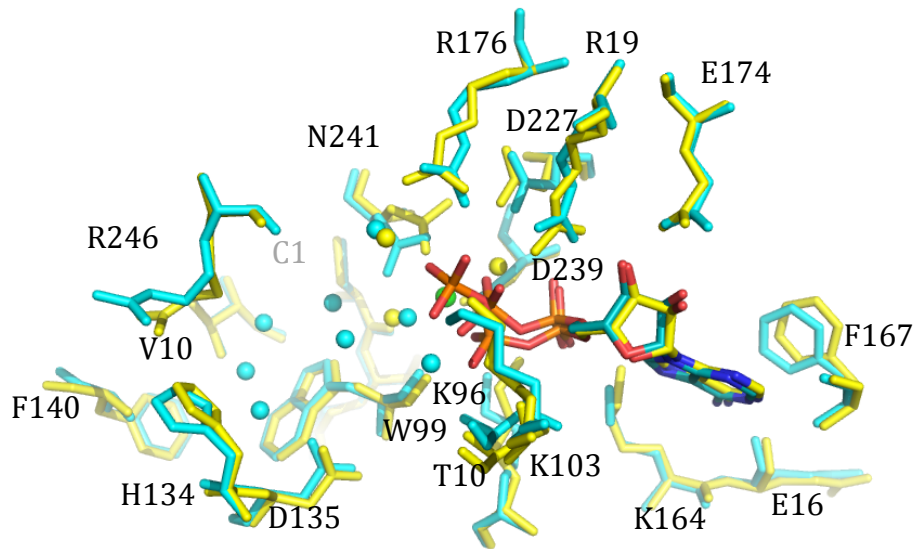


**Figure S5: Binding of ATP in Sp-cdc123:Sc-eIF2γDIII complex**

A- View of the 2.9 Å 'mFo-DFc' map of the Sp-cdc123:Sc-eIF2γDIII complex contoured at 1.0 standard deviation. Magnesium ion and water molecules are shown as green and red spheres, respectively. The view shows the coordination sphere of the magnesium ion involving the three highly conserved residues D227, D239 and N241 (Figure S1). B- Superimposition of the Sp-Cdc1223ΔC:ADP structure on that of Sp-cdc123:Sc-eIF2γDIII:ATP-Mg<sup>2+</sup> structure. Residues of Sp-

cdc123:Sc-eIF2 $\gamma$ DIII:ATP-Mg<sup>2+</sup> are colored in yellow and those of Sp-Cdc1223 $\Delta$ C:ADP are in cyan.

Magnesium ion is shown as a green sphere and water molecules as yellow and cyan spheres.

1  
2  
3  
4  
5  
6  
7  
8  
9  
10  
11  
12  
13  
14  
15  
16  
17  
18  
19  
20  
21  
22  
23  
24  
25  
26  
27  
28  
29  
30  
31  
32  
33  
34  
35  
36  
37  
38  
39  
40  
41  
42  
43  
44  
45  
46  
47  
48  
49  
50  
51  
52  
53  
54  
55  
56  
57  
58  
59  
60  
61  
62  
63  
64  
65

1  
2  
3  
4  
5  
6  
7  
8  
9  
10  
11  
12  
13  
14  
15  
16  
17  
18  
19  
20  
21  
22  
23  
24  
25  
26  
27  
28  
29  
30  
31  
32  
33  
34  
35  
36  
37  
38  
39  
40  
41  
42  
43  
44  
45  
46  
47  
48  
49  
50  
51  
52  
53  
54  
55  
56  
57  
58  
59  
60  
61  
62  
63  
64  
65

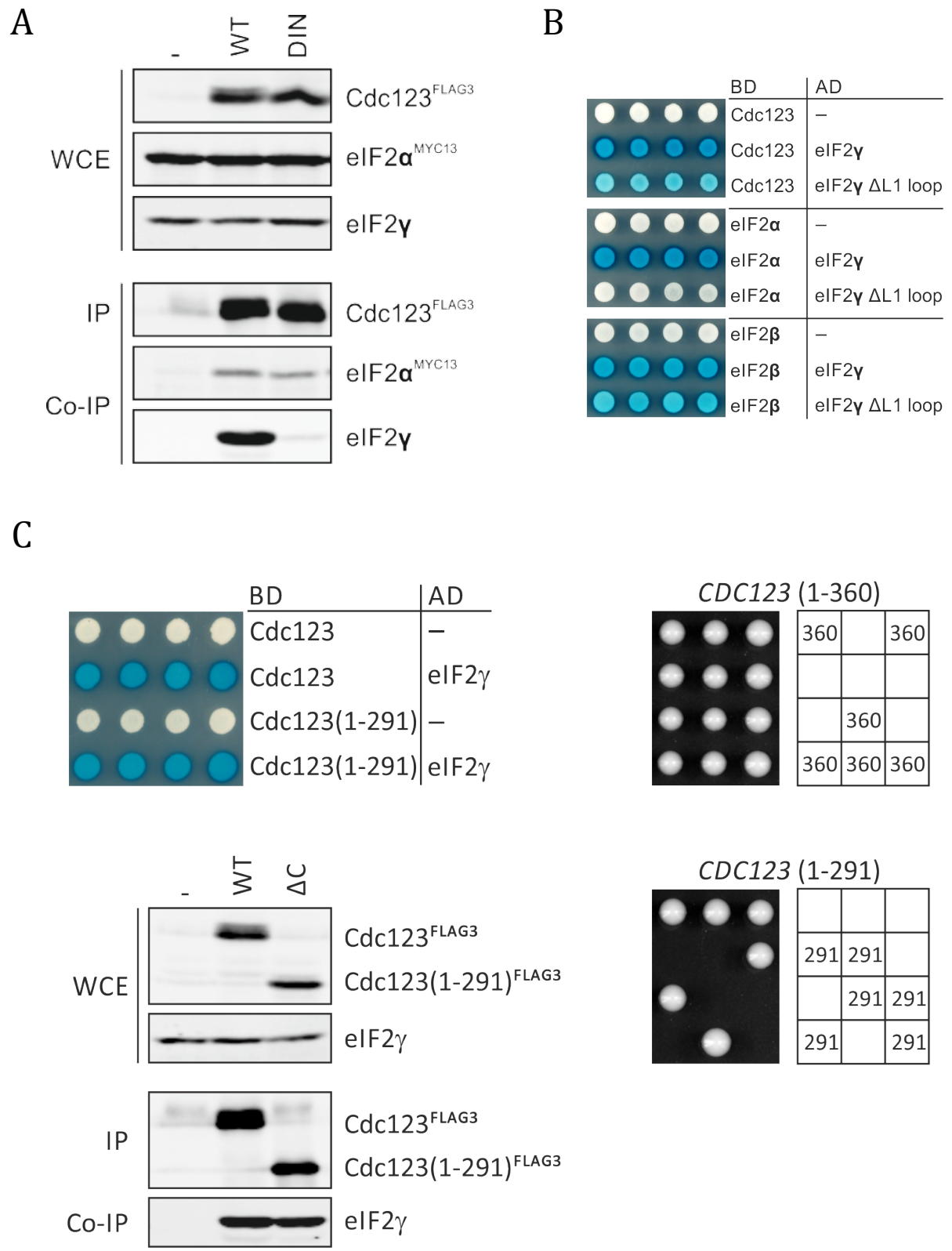


**Figure S6: Interaction of Sc-Cdc123 with eIF2 subunits and role of the C-terminal domain**

1  
2 A- Interaction of Cdc123 with eIF2 $\alpha$  and  $\gamma$  subunits.  
3

4 Immunoprecipitates of Cdc123 and Cdc123-DIN were analyzed for co-precipitation of eIF2 $\alpha$  and  
5 eIF2 $\gamma$  in yeast strains that express a myc-tagged version of eIF2 $\alpha$  and overexpresses from the *TEF2*  
6 promoter a flag-tagged version of Cdc123 (WT) (W14185) or Cdc123-DIN (DIN) (W14186). A strain  
7 that expresses a myc-tagged version of eIF2 $\alpha$  but lacks a flag-tagged version of Cdc123 (-) (W9876)  
8 was included as a negative control. Protein levels were determined by Western analysis in yeast whole  
9 cell extracts (WCE). Immunoprecipitates (IP) of Cdc123-flag and Cdc123-DIN-flag were prepared  
10 and analyzed for the presence of eIF2 $\alpha$  and eIF2 $\gamma$  (Co-IP). For precipitation and detection of Cdc123-  
11 flag and Cdc123-DIN-flag the mouse monoclonal antibody M2 was used. eIF2 $\alpha$ -myc and eIF2 $\gamma$  were  
12 detected by the mouse monoclonal antibody 9E10 and a rabbit antiserum to eIF2 $\gamma$  (Perzlsmaier et al.,  
13 2013), respectively. Relative to eIF2 $\gamma$ , much lower amounts of eIF2 $\alpha$  co-precipitated with Cdc123.  
14 The DIN mutation of Cdc123 reduced the interaction of Cdc123 with eIF2 $\gamma$ , but had little or no effect  
15 on the interaction of Cdc123 with eIF2 $\alpha$ .  
16  
17  
18  
19  
20  
21  
22  
23  
24  
25  
26  
27  
28  
29  
30  
31

32 B- Role of the L1 loop of eIF2 $\gamma$  in the interaction of eIF2 $\gamma$  with Cdc123, eIF2 $\alpha$  and eIF2 $\beta$ .  
33

34 A yeast-two-hybrid assay was used to evaluate the consequences of deleting part of the L1 loop of  
35 eIF2 $\gamma$  (Sc-eIF2 $\gamma$ /Gcd11 aa325-331) on the ability of eIF2 $\gamma$  to associate with Cdc123 and eIF2 subunits.  
36 The reporter strain W276 was co-transformed with the indicated combination of a pEG202-derived  
37 DNA binding domain (BD) plasmid (BD-Cdc123: pWS1463; BD-eIF2 $\alpha$ : pWS1537; BD-eIF2 $\beta$ :  
38 pWS1535) and a pJG4-5-derived transcriptional activation domain (AD) plasmid (AD -: pJG4-5; AD-  
39 eIF2 $\gamma$ : pWS1513; AD-eIF2 $\gamma$   $\Delta$ L1 loop: pED002). The yeast-two-hybrid vector plasmids pEG202 and  
40 pJG4-5 have been described (Ausubel et al., 2005). Yeast colonies were overlaid with an X-gal top  
41 agar to visualize  $\beta$ -galactosidase reporter activation. The L1 loop deletion of eIF2 $\gamma$  reduced the  
42 interaction of eIF2 $\gamma$  with Cdc123 and prevented any interaction with eIF2 $\alpha$ , but had little or no effect  
43 on the interaction with eIF2 $\beta$ .  
44  
45  
46  
47  
48  
49  
50  
51  
52  
53  
54  
55  
56  
57

58 C- Role of the C-terminal domain of Cdc123  
59  
60  
61  
62  
63  
64  
65

1 A C-terminal truncation mutant of Cdc123 (Cdc123(1-291) lacking 69 amino acids from the C-  
2 terminus) was analyzed for its ability to interact with eIF2 $\gamma$  and support cell viability.

3  
4 Left upper panel- Yeast-two-hybrid analysis of the Cdc123-eIF2 $\gamma$  interaction. The reporter strain  
5 W276 was co-transformed with the indicated combination of a pEG202-derived DNA binding domain  
6 (BD) plasmid (BD-Cdc123: pWS1463; BD-Cdc123(1-291): pWS3801) and a pJG4-5-derived  
7 transcriptional activation domain (AD) plasmid (AD -: pJG4-5; AD-eIF2 $\gamma$ : pWS1513). The yeast-two-  
8 hybrid vector plasmids pEG202 and pJG4-5 have been described (Ausubel et al., 2005). Yeast  
9 colonies were overlaid with an X-gal top agar to visualize  $\beta$ -galactosidase reporter activation.

10  
11 Left lower panel- Co-immunoprecipitation analysis of the Cdc123-eIF2 $\gamma$  interaction. Strains  
12 expressing flag-tagged versions of Cdc123 (WT; W14236) or Cdc123(1-291) ( $\Delta$ C; W14237) from the  
13 regulable *GALI* promoter were used for preparation of whole cell extracts (WCE), anti-flag  
14 immunoprecipitation (IP) and analysis of co-precipitation (Co-IP) of eIF2 $\gamma$ . A strain lacking a flag-  
15 tagged version of Cdc123 (-; W9878) was used as a negative control. Cdc123-flag, Cdc123(1-291)-  
16 flag and eIF2 $\gamma$  protein levels were detected by Western analysis of whole cell extracts (WCE).

17  
18 Cdc123-flag and Cdc123(1-291)-flag were immunoprecipitated (IP) and detected with the mouse  
19 monoclonal flag antibody M2. The precipitates were analyzed for co-precipitation of eIF2 $\gamma$  (Co-IP)  
20 using a rabbit antiserum to eIF2 $\gamma$  (Perzmaier et al., 2013).

21  
22 Right panels- Tetrad dissection analysis for evaluating the biological function of Cdc123(1-291).  
23 Diploid yeast cells heterozygote for a C-terminal HA3-fusion of either wild-type *CDC123* (upper  
24 panel; W14233) or C-terminal truncation mutant *CDC123(1-291)* (lower panel; W2880) were  
25 sporulated and subjected to tetrad dissection.

26  
27 The C-terminal truncation of Cdc123 had no effect on the interaction of Cdc123 with eIF2 $\gamma$ , but  
28 disrupted the biological function of Cdc123.  
29  
30  
31  
32  
33  
34  
35  
36  
37  
38  
39  
40  
41  
42  
43  
44  
45  
46  
47  
48  
49  
50  
51  
52  
53  
54  
55  
56  
57  
58  
59  
60  
61  
62  
63  
64  
65

## Supplemental Table

	Full-length cdc123 <sup>a</sup>	Full-length cdc123 <sup>a</sup>	Full-length cdc123 Se-met
<b>Data collection</b>			
Crystallization Conditions	22.5% PEG3350 20mM (NH <sub>4</sub> ) <sub>2</sub> C <sub>4</sub> H <sub>4</sub> O <sub>6</sub> +ATP-Mg <sup>2+</sup>	22.5% PEG3350 20mM(NH <sub>4</sub> ) <sub>2</sub> C <sub>4</sub> H <sub>4</sub> O <sub>6</sub>	20%PEG3350 0.1M NH <sub>4</sub> F
Space group	P2 <sub>1</sub> 2 <sub>1</sub> 2 <sub>1</sub>	C222	C222
Cell dimensions			
<i>a, b, c</i> (Å)	87.69 100.19 129.68	87.17 208.07 87.45	86.42 295.6 86.00
<i>a, b, γ</i> (°)	90 90 90	90 90 90	90 90 90
Molecules in a.u	4	2	2
Resolution (Å)	49.1-3.0	49.10-3.24	49.4-5.5
<i>R</i> <sub>sym</sub>	10.5 (135.0) <sup>b</sup>	4.8 (71.1)	7.6 (42.1)
<i>I</i> / <i>σI</i>	13.55 (1.29)	19.68 (2.42)	23.01 (6.85)
CC1/2	99.9 (61.2)	99.9 (81.3)	99.9 (97.3)
Completeness (%)	99.9 (99.8)	96.8 (95.9)	99.8 (100)
Redundancy	7.3 (7.4)	5.51 (5.50)	14.36 (14.88)
sigAno			1.671 (0.943)
Ano. Correlation (%)			57 (23)

**Table S1:** Data collection statistics for Sp-cdc123 structure resolution

<sup>a</sup>A single crystal was used for data collection.

<sup>b</sup>Values in parentheses are for highest-resolution shell.

## Supplemental Experimental Procedures

### Protein expression and purification

#### *Sc-γDIII*

*Sc-γDIII* domain was purified from 1 liter of culture of BL21 Rosetta *E. coli* cells transformed with pET3a-*Sc-γDIII*. The pellet was resuspended in buffer A. After sonication and centrifugation, the extract was loaded onto an S-Sepharose column (16mm x 20cm; GE-Healthcare) equilibrated in buffer A. A gradient from 200 mM NaCl to 1 M NaCl was used for elution (300 mL at a flow rate of 2.5

1 mL/min). The recovered fractions were pooled, concentrated and loaded onto a Superdex 200 HR 10/30 column equilibrated in buffer A. The purified protein was concentrated to 10 mg/mL.

2  
3  
4 An N-terminally tagged version of Sc- $\gamma$ DIII domain was purified from BL21 Rosetta *E. coli*  
5  
6 cells transformed with PWS3915 and induced with 0.2% rhamnose after overnight culture at 37°C.  
7  
8 The same purification protocol as the one described above was used for the purification except that a  
9  
10 first step of affinity chromatography was added. The resulting protein was used to perform titration  
11  
12 experiments using isothermal calorimetry (ITC).  
13  
14  
15

### 16 17 18 *Sc-Cdc123*

19  
20 Plasmid pWS1389 allows expression of an N-terminally his-tagged version of Sc-Cdc123.  
21  
22 The plasmid was transformed into BL21 Rosetta *E. coli* cells. Overexpression of Sc-Cdc123 was  
23  
24 induced with 0.2% rhamnose after overnight culture at 37°C. After induction, the culture was  
25  
26 continued for 4 hours at 18°C. The cells were resuspended in buffer B. After sonication and  
27  
28 centrifugation, the crude extract was loaded onto a column (4 mL) containing Talon affinity resin  
29  
30 (Clontech) equilibrated in buffer B. Sc-Cdc123 was eluted with buffer B containing 125 mM  
31  
32 imidazole. After dialysis against buffer C (10 mM HEPES pH 7.5, 100 mM NaCl, 3 mM 2-  
33  
34 mercaptoethanol, 0.1 mM PMSF, 0.1 mM benzamidine), the protein was loaded onto a Q-Sepharose  
35  
36 column (0.8 mm x 3 cm; GE-Healthcare) equilibrated in buffer C. A gradient from 100 mM NaCl to  
37  
38 600 mM NaCl was used for elution (60 mL at a flow rate of 2mL/min). The recovered protein was  
39  
40 finally concentrated and loaded onto a Superdex 200 column (HR 10/30; GE Healthcare) equilibrated  
41  
42 in buffer A. Fractions containing Sp-Cdc123:Sc- $\gamma$ DIII were pooled and concentrated to 10 mg/mL.  
43  
44  
45  
46  
47  
48

### 49 **SAXS data collection**

50  
51 SAXS experiments were conducted on beamline SWING at the SOLEIL Synchrotron ( $\lambda =$   
52  
53 1.033 Å). The Avix charge-coupled device detector was positioned at a distance of 2076 mm from  
54  
55 the sample, with the direct beam off-centered. Data were collected in the  $Q$ -range 0.008–0.5 Å<sup>-1</sup> ( $Q =$   
56  
57  $4\pi\sin\theta/\lambda$ ,  $2\theta$  is the scattering angle). All solutions were circulated in a thermostated (15 °C) quartz  
58  
59  
60  
61  
62  
63  
64  
65

1 capillary with a diameter of 1.5 mm and a wall thickness of 10  $\mu\text{m}$ , positioned within a vacuum  
2 chamber.

3  
4 For data collection purified complex Sp-Cdc123- $\gamma$ DIII (*c.a* 20 nanomoles in 100-200  $\mu\text{l}$ ) was  
5 injected on a size-exclusion column (Agilent $\text{\textcircled{C}}$  BioSEC 3-300) using an Agilent $\text{\textcircled{C}}$  High Performance  
6 Liquid Chromatography system and eluted directly into the SAXS flow-through capillary cell at a  
7 flow rate of 0.2 mL/min. The elution buffer was 10 mM Hepes pH 7.5, 500 mM NaCl. SAXS data  
8 were collected online, with a frame duration of 1.5 s and a dead time between frames of 1.0 s. A large  
9 number of frames were collected during the first minutes of the elution and averaged to account for  
10 buffer scattering, which was subsequently subtracted from the signal during elution of the protein  
11 complex. Selected curves corresponding to the main elution peak were averaged on the basis of  
12 identical shapes (David and Perez, 2009). Data reduction to absolute units, frame averaging and  
13 subtraction, were performed using FOXTROT ([http://www.synchrotron-](http://www.synchrotron-soleil.fr/Recherche/LignesLumiere/SWING)  
14 [soleil.fr/Recherche/LignesLumiere/SWING](http://www.synchrotron-soleil.fr/Recherche/LignesLumiere/SWING)). All subsequent data processing, analysis, and modeling  
15 steps were carried out with PRIMUS and other programs of the ATSAS suite (Konarev et al., 2006).  
16 Scattered intensity curves were calculated from the atomic coordinates of the crystallographic  
17 structures using CRY SOL (Svergun et al., 1995) with 50 harmonics. This program was also used to fit  
18 the calculated curve to the experimental one, by adjusting the excluded volume, the averaged atomic  
19 radius and the contrast of the hydration layer surrounding the particle in solution.  
20  
21  
22  
23  
24  
25  
26  
27  
28  
29  
30  
31  
32  
33  
34  
35  
36  
37  
38  
39  
40  
41

#### 42 **Pull-Down assays**

43  
44 A 15 mL culture of wt-Sc- $\gamma$ DIII or mutant Sc- $\gamma$ DIII (E460A, R504A, W509A) was mixed to a  
45 15 mL culture of N-terminally tagged version of Sp-Cdc123, centrifugated and resuspended in 1 mL  
46 of buffer B. After sonication, the insoluble fraction was removed by centrifugation. The crude extract  
47 was then mixed with 200  $\mu\text{L}$  of metal affinity resin (Talon, Clontech) to perform batch purification.  
48 After several rounds of beads washing, the retained complex was eluted from the resin with buffer B  
49 supplemented with 125 mM imidazole. A fixed volume aliquot of each step of the batch purification  
50 was loaded onto a 12% polyacrylamide SDS gel (Figure S4).  
51  
52  
53  
54  
55  
56  
57  
58  
59  
60  
61  
62  
63  
64  
65

## ITC

### *Binding of $\gamma$ DIII*

Before ITC measurements, proteins were dialyzed against buffer B. Titrations curves were obtained using a MicroCal200 apparatus (Malvern). Sc-Cdc123 (250  $\mu$ L, 20  $\mu$ M) was titrated by 20 injections (4  $\mu$ L) of Sc- $\gamma$ DIII at a concentration of 150  $\mu$ M. A typical titration curve is shown in Figure S3C. The deduced dissociation constant for the Sc- $\gamma$ DIII:Sc-Cdc123 complex was  $2.5 \pm 0.5$   $\mu$ M.

### *Binding of ATP*

Before ITC measurements proteins were dialyzed against buffer A supplemented with 5 mM  $MgCl_2$ . Titrations curves were obtained using a MicroCal200 apparatus (Malvern). 250  $\mu$ L of Sp-Cdc123 or of Sp-Cdc123- $\gamma$ DIII complex, (125  $\mu$ M) was titrated by 20 injections (4  $\mu$ L) of ATP at a concentration of 1.25 mM. A typical titration curve is shown in Figure S3A. The deduced dissociation constant were similar for the Sc-Cdc123:ATP- $Mg^{2+}$  complex ( $67 \pm 13$   $\mu$ M) and for the Sc-Cdc123- $\gamma$ DIII:ATP- $Mg^{2+}$  complex ( $57 \pm 7$   $\mu$ M). Reported results are mean  $\pm$  s.d. from at least two independent experiments.

## Yeast methods

For growth, transformation, mating, sporulation, and tetrad dissection of budding yeast cells, standard protocols were followed (Ausubel et al., 2005). Yeast strains used in this study are isogenic derivatives of W303 and listed below. Cells were grown in YEP complex medium containing adenine (100 mg/L), tryptophan (200 mg/L),  $KH_2PO_4$  (10 mM), and glucose (2%) or raffinose (2%). To induce expression from the *GALI* promoter, 2% galactose was added to YEP complex medium containing raffinose.

strain	relevant genotype	figure
W276	<i>MATa his3 trp1 ura3::lexA-op-lacZ-URA3 leu2::lexA-op-LEU2</i>	S9, S11
W2880	<i>MATa/α CDC123/CDC123(1-291)-HA3-HIS3MX6</i>	S11
W7743	<i>MATa CDC123 trp1::pTEF2-3xFLAG-GCD11-tCYC1-TRP1 ura3::pTEF2-SUI2-tCYC1-URA3</i>	5B
W7745	<i>MATa cdc123-delta::kanMX4 trp1::pTEF2-3xFLAG-GCD11-tCYC1-TRP1 ura3::pTEF2-SUI2-tCYC1-URA3</i>	5B
W9876	<i>MATa/α SUI2/SUI2-MYC13-HIS3MX6</i>	S10
W9878	<i>MATa ura3</i>	S11
W13930	<i>MATa cdc123-delta::kanMX4 trp1::pTEF2-3xFLAG-GCD11-tCYC1-TRP1 ura3::pTEF2-SUI2-tCYC1-URA3 leu2::pCDC123-CDC123-tCYC1-LEU2</i>	5B
W13931	<i>MATa cdc123-delta::kanMX4 trp1::pTEF2-3xFLAG-GCD11-tCYC1-TRP1 ura3::pTEF2-SUI2-tCYC1-URA3 leu2::pCDC123-CDC123DIN-tCYC1-LEU2</i>	5B
W13935	<i>MATa/α CDC123/cdc123-delta::kanMX4 pCDC123-CDC123D252A-tCYC1-URA3 (ARS/CEN)</i>	5B
W13936	<i>MATa/α CDC123/cdc123-delta::kanMX4 pCDC123-CDC123DIN(266-268)-tCYC1-URA3 (ARS/CEN)</i>	5B
W14145	<i>MATa/α CDC123/cdc123-delta::kanMX4 pCDC123-CDC123-tCYC1-URA3 (ARS/CEN)</i>	5B
W14185	<i>MATa/α SUI2/SUI2-MYC13-HIS3MX6 ura3/ura3::pTEF2-CDC123-FLAG3-tCYC1-URA3</i>	S10
W14186	<i>MATa/α SUI2/SUI2-MYC13-HIS3MX6 ura3/ura3::pTEF2-CDC123DIN-FLAG3-tCYC1-URA3</i>	S10
W14233	<i>MATa/α CDC123/CDC123-HA3-HIS3MX6</i>	S11
W14236	<i>MATa ura3::pGAL1-CDC123-FLAG3-tCYC1-URA3</i>	S11
W14237	<i>MATa ura3::pGAL1-CDC123(1-291)-FLAG3-tCYC1-URA3</i>	S11
W14238	<i>MATa cdc123-delta::kanMX4 trp1::pTEF2-3xFLAG-GCD11-tCYC1-TRP1 ura3::pTEF2-SUI2-tCYC1-URA3 leu2::pCDC123-CDC123D252A-tCYC1-LEU2</i>	5B

Yeast strains

### DNA constructs and genetic manipulation

Yeast plasmid constructs used in this study are derivatives of pRS vectors (Sikorski and Hieter, 1989), pEG202 or pJG4-5 (Ausubel et al., 2005) and are listed below. C-terminal epitope fusions of endogenous genes and the C-terminal truncation of *CDC123* (*CDC123(1-291)*) were constructed by PCR-based epitope tagging (Longtine et al., 1998). Site-directed mutagenesis (Quick-change; Stratagene) was used to replace the D266, I267, N268, and D252 codons of *CDC123* by alanine codons.

<b>name</b>	<b>description</b>	<b>vector</b>	<b>figure</b>
pED002	<i>pGAL-NLS-AD-HA-GCD11-delta L1 loop(delta325-331)</i>	pJG4-5	S9
pJG4-5	<i>pGAL-NLS-AD-HA-MCS, TRP1, 2μ</i>		S9, S11
pWS1378	<i>pCDC123-CDC123-tCYC1, ARS/CEN</i>	pRS416	5B
pWS1463	<i>pADH-lexA-CDC123</i>	pEG202	S9, S11
pWS1513	<i>pGAL-NLS-AD-HA-GCD11</i>	pJG4-5	S9, S11
pWS1535	<i>pADH-lexA-SUI3</i>	pEG202	S9
pWS1537	<i>pADH-lexA-SUI2</i>	pEG202	S9
pWS1846	<i>pCDC123-CDC123-tCYC1</i>	pRS305	5B
pWS3801	<i>pADH-lexA-CDC123(1-291)</i>	pEG202	S11
pWS4398	<i>pCDC123-CDC123D252A-tCYC1, ARS/CEN</i>	pRS416	5B
pWS4399	<i>pCDC123-CDC123D266A/I267A/N268A-tCYC1, ARS/CEN</i>	pRS416	5B
pWS4465	<i>pCDC123-CDC123D266A/I267A/N268A-tCYC1</i>	pRS305	5B
pWS4488	<i>pTEF2-CDC123-FLAG3-tCYC1</i>	pRS306	S10
pWS4501	<i>pTEF2-CDC123D266A/I267A/N268A -FLAG3-tCYC1</i>	pRS306	S10
pWS4671	<i>pCDC123-CDC123D252A-tCYC1</i>	pRS305	5B
pWS4677	<i>pGAL1-CDC123-FLAG3-tCYC1</i>	pRS306	S11
pWS4678	<i>pGAL1-CDC123(1-291)-FLAG3-tCYC1</i>	pRS306	S11

Yeast plasmids

### Yeast-Two-Hybrid assay

The Y2H reporter strain W276 was co-transformed with pEG202 and pJG4-5 derivatives. Transformants were spotted on synthetic complete solid medium lacking histidine and tryptophan and containing saccharose (1%) and galactose (2%). Plates were incubated over night at 30°C.  $\beta$ -galactosidase activity was visualized by overlaying the yeast colonies with an X-gal top agar containing sodium phosphate buffer (0.5 M, pH 7.0), DMFA (6%), X-Gal (0.2 mg/ml), SDS (0.1%), and Bacto agar (0.5%). Coloration was documented after incubation over night at 30°C.

### Yeast cell extracts, immunoprecipitation and Western analysis

Whole cell protein extracts and immunoprecipitations were made as described (Arnold et al., 2015; Perzmaier et al., 2013). SDS-PAGE and Western analysis were done essentially as described (Schwab et al., 2001). Mouse monoclonal antibodies M2 (Sigma-Aldrich) and 9E10 were used for detection of FLAG-tagged and MYC-tagged proteins, respectively. eIF2 $\alpha$  (Sui2), eIF2 $\gamma$  (Gcd11), and Cdc123 were detected using a polyclonal rabbit antiserum (Sui2) or affinity-purified polyclonal rabbit antisera (Gcd11, Cdc123) (Perzmaier et al., 2013). Detection of immunoblots was done using IRDye secondary antibodies and an Odyssey infrared imaging system (LI-COR Biosciences).

## Supplemental references

- Ausubel FM, Brent R, Kingston RE, Moore DD, Seidman JG, Smith JA, Struhl K (2005) *Current Protocols in Molecular Biology*: John Wiley & Sons, Inc.
- Arnold, L., Hockner, S., and Seufert, W. (2015). Insights into the cellular mechanism of the yeast ubiquitin ligase APC/C-Cdh1 from the analysis of in vivo degrons. *Mol Biol Cell* *26*, 843-858.
- Ausubel, F.M., Brent, R., Kingston, R.E., Moore, D.D., Seidman, J.G., Smith, J.A., and Struhl, K. (2005). *Current Protocols in Molecular Biology* (John Wiley & Sons, Inc.).
- David, G., and Perez, J. (2009). combined sampler robot and high-performance liquid chromatography: a fully automated system for biological small-angle X-ray scattering experiments at the Synchrotron SOLEIL SWING beamline. *J Appl Crystallogr* *42*, 892-900.
- Gouet, P., Courcelle, E., Stuart, D.I., and Metoz, F. (1999). ESPript: analysis of multiple sequence alignments in PostScript. *Bioinformatics* *15*, 305-308.
- Konarev, P.V., Volkov, V.V., Petoukhov, M.V., and Svergun, D.I. (2006). ATSAS 2.1, a program package for small-angle scattering data analysis. *J Appl Crystallogr* *39*, 277-286.
- Larkin, M., Blackshields, G., Brown, N., Chenna, R., McGettigan, P., McWilliam, H., Valentin, F., Wallace, I., Wilm, A., Lopez, R., *et al.* (2007). ClustalW and ClustalX version 2 *Bioinformatics* *23*, 2947-2948.
- Longtine, M.S., McKenzie, A., 3rd, Demarini, D.J., Shah, N.G., Wach, A., Brachet, A., Philippsen, P., and Pringle, J.R. (1998). Additional modules for versatile and economical PCR-based gene deletion and modification in *Saccharomyces cerevisiae*. *Yeast* *14*, 953-961.
- Miles, B.W., Thoden, J.B., Holden, H.M., and Raushel, F.M. (2002). Inactivation of the amidotransferase activity of carbamoyl phosphate synthetase by the antibiotic acivicin. *J Biol Chem* *277*, 4368-4373.
- Miller, G.J., Wilson, M.P., Majerus, P.W., and Hurley, J.H. (2005). Specificity determinants in inositol polyphosphate synthesis: crystal structure of inositol 1,3,4-trisphosphate 5/6-kinase. *Mol Cell* *18*, 201-212.
- Ouchi, T., Tomita, T., Horie, A., Yoshida, A., Takahashi, K., Nishida, H., Lassak, K., Taka, H., Mineki, R., Fujimura, T., *et al.* (2013). Lysine and arginine biosyntheses mediated by a common carrier protein in *Sulfolobus*. *Nature chemical biology* *9*, 277-283.
- Perzmaier, A.F., Richter, F., and Seufert, W. (2013). Translation initiation requires cell division cycle 123 (Cdc123) to facilitate biogenesis of the eukaryotic initiation factor 2 (eIF2). *J Biol Chem* *288*, 21537-21546.
- Roper, D.I., Huyton, T., Vagin, A., and Dodson, G. (2000). The molecular basis of vancomycin resistance in clinically relevant Enterococci: crystal structure of D-alanyl-D-lactate ligase (VanA). *Proc Natl Acad Sci U S A* *97*, 8921-8925.
- Schwab, M., Neutzner, M., Mocker, D., and Seufert, W. (2001). Yeast Hct1 recognizes the mitotic cyclin Clb2 and other substrates of the ubiquitin ligase APC. *EMBO J* *20*, 5165-5175.
- Sikorski, R.S., and Hieter, P. (1989). A system of shuttle vectors and yeast host strains designed for efficient manipulation of DNA in *Saccharomyces cerevisiae*. *Genetics* *122*, 19-27.
- Svergun, D.I., Barberato, C., and Koch, M.H.J. (1995). CRYSOLE - a program to evaluate X-ray solution scattering of biological macromolecules from atomic coordinates. *J Appl Crystallogr* *28*, 768-773.
- Thoden, J.B., Firestine, S., Nixon, A., Benkovic, S.J., and Holden, H.M. (2000). Molecular structure of *Escherichia coli* PurT-encoded glycinamide ribonucleotide transformylase. *Biochemistry* *39*, 8791-8802.
- Waterhouse, A., Procter, J., Martin, D., Clamp, M., and Barton, G. (2009). Jalview Version 2 - a multiple sequence alignment editor and analysis workbench. *Bioinformatics* *25*, 1189-1191.
- Yatime, L., Mechulam, Y., Blanquet, S., and Schmitt, E. (2006). Structural switch of the gamma subunit in an archaeal aIF2 alpha gamma heterodimer. *Structure* *14*, 119-128.
- Zhao, G., Jin, Z., Wang, Y., Allewell, N.M., Tuchman, M., and Shi, D. (2013). Structure and function of *Escherichia coli* RimK, an ATP-grasp fold, L-glutamyl ligase enzyme. *Proteins* *81*, 1847-1854